Journal of Power Sources 219 (2012) 339–357

Contents lists available at SciVerse ScienceDirect

Journal of Power Sources

journal homepage: www.elsevier.com/locate/jpowsour

Review

Developments in direct borohydride fuel cells and remaining challenges

I. Merino-Jiménez [a], C. Ponce de León [a,*], A.A. Shah [b], F.C. Walsh [a]

[a] Electrochemical Engineering Laboratory, Energy Technology Research Group, Engineering Sciences, University of Southampton, Highfield Rd., Southampton SO17 1BJ, UK
[b] School of Engineering, University of Warwick, Coventry CV4 7AL, UK

HIGHLIGHTS

- We review aspects of the borohydride fuel cell that have not been revised previously.
- Aspects of the borohydride hydrolysis, modelling, simulation and recycling are discussed.
- Future trends and recommendations to improve the technology are suggested

ARTICLE INFO

Article history:
Received 27 April 2012
Received in revised form
13 June 2012
Accepted 27 June 2012
Available online 17 August 2012

Keywords:
Direct borohydride fuel cells
Hydrolysis inhibition
Mathematical modelling
Membranes
Surfactants
Recycling

ABSTRACT

Over the last twenty years, there has been a resurgent research interest in direct borohydride fuel cells (DBFCs) highlighting the fundamental aspects that need to be addressed to achieve their optimal performance. The main problem is the hydrolysis of borohydride ions, which generates hydrogen, decreases the energy efficiency and reduces the power density. The electrons released during borohydride oxidation, the cell potential difference and the power output are strongly influenced by the choice of anode and cathode, including three-dimensional and nanostructured electrodes, the electrolyte composition and the operating conditions. Extensive investigations on various anodic electrocatalysts and their effect on the oxidation and hydrolysis have been quantified as well as the cathode catalyst and its influence on the overall fuel cell performance. Computational methods such as ab-initio and physical modelling could play prominent roles in the design and fundamental characterisation of DBFCs but are currently underused and only small number of studies in well-defined materials such as Pt (111) or Au (111) exist. Cell design and configuration have also been considered but the basic requirement to engineer a selective catalyst able to suppress the hydrogen evolution and the elucidation of the mechanism of borohydride ion oxidation, remain.

1. Introduction

Fuel cells offer a promising alternative to incumbent electrical power generation technologies (primarily based on fossil fuels), for medium-scale applications such as remote or backup power, as well as small-scale applications, such as portable consumer electronics. Widespread adoption of the direct hydrogen-oxygen fuel cell, the most highly-developed fuel cell, is hindered by a number of problems related to the sourcing, storage and safe handling of hydrogen (particularly for mobile applications) [1]. Fuel reformers integrated with fuel cell stacks can generate the hydrogen from hydrocarbon fuels but present additional engineering complications and add further volume, weight and cost to the overall power system. An alternative solution to the aforementioned issues is the replacement of gaseous hydrogen with a liquid hydrogen carrier, often an alcohol such as ethanol or methanol. The latter leads to the direct methanol fuel cell (DMFC), which, on the other hand, suffers from high rates of reactant crossover and low power densities. Other hydrogen-containing compounds under consideration are metal hydrides (in solution), such as $LiBH_4$, $NaBH_4$ or KBH_4 [2]. Table 1 shows the theoretical energy densities for different fuels and oxidants. Comparing these values, the maximum corresponds to the $NaBH_4/H_2O_2$ system (up to 17 kW h kg^{-1}), followed by the $NaBH_4/O_2$ system (up to 9.3 kW h kg^{-1}). The theoretical energy density of a $NaBH_4/H_2O_2$ cell is at least five-fold that of a H_2/O_2 fuel cell, two-fold that of an ethanol/O_2 cell and three-fold that of a methanol/O_2 cell.

The direct borohydride fuel cell (DBFC) has been studied since 1960, when Pt and Ni were investigated by Elder and Hickling [3] and Indig and Snyder [4], respectively, as anode catalysts for borohydride oxidation. Fig. 1 shows a histogram of the number of papers published on the DBFC and the reactions of borohydride

* Corresponding author. Tel.: +44 0 23 8059 8931/6727; fax: +44 0 23 8059 7051.
E-mail address: capla@soton.ac.uk (C. Ponce de León).

0378-7753/$ – see front matter © 2012 Elsevier B.V. All rights reserved.
http://dx.doi.org/10.1016/j.jpowsour.2012.06.091

Abbreviations

CE	Chemical electrochemical
DBFC	Direct borohydride fuel cell
DCEF	Direct charging electrostatic flocking
DFT	Density functional theory
ECE	Electrochemical chemical electrochemical
FeTMPP	Iron tetramethoxylphenyl prophyrin
IBFC	Indirect borohydride fuel cell
MEA	Membrane electrode assembly
MMO	Mercury/mercury oxide
NRE-212	Untreated Nafion membrane
OCP	Open circuit potential
PEM	Proton electrolyte membrane
PAHM	Polyvinyl alcohol hydrogel membrane
RHE	Reversible hydrogen electrode
RN	Reticulated nickel
RVC	Reticulated vitreous carbon
SCE	Saturated calomel electrode
SHE	Standard hydrogen electrode
TEAH	Tetraethyl ammonium hydroxide
TU	Thiourea

Symbols

E	Electrode potential V
E_{cell}	Cell potential V
E^0_{cell}	Open-circuit potential V
I	Current A
P	Power density W cm^{-2}
R	Electrical resistance Ω
η_{act}	Activation overpotential V
η_{conc}	Concentration overpotential V

oxidation and borohydride hydrolysis. An increased interest in the field over the last ten years is clearly apparent from this plot. The number of publications on direct borohydride fuel cells maintained an average of 54 papers per year between 2007 and 2011, which confirms the high degree of interest in the technology. Much of the focus has been placed on the hydrolysis of borohydride ions [5], due to its relevance to both direct and indirect borohydride fuel cells (in the indirect borohydride fuel cell (IBFC), pure hydrogen is generated by hydrolysis and fed into a hydrogen/oxygen fuel cell). Indeed, the number of publications on borohydride hydrolysis is slightly higher than that of the DBFC itself.

Table 2 presents a summary of the direct borohydride fuel cells reviews published over the last ten years. In 2006, Ponce de Leon et al. [1] published an extended review of the DBFC, which was followed by two reviews in 2009 that included information on fuel cell developments and the main technical and economic challenges faced by the technology [6,7]. In 2010, Ma et al. [8] published the most recent review describing the anode and cathode materials used in DBFC, the use of different membranes and the effect of operating conditions on fuel cell performance. There have been a number of notable developments since the review by Ma et al., particularly on different anode materials and improvements in the cell design, together with the development of mathematical models, all of which are detailed in this review. In light of these recent advances, the remaining open challenges and their potential solutions are highlighted and discussed in detail in the remaining sections.

1.1. Cell performance

The cell potential of a fuel cell deviates from the theoretical, reversible open-circuit potential difference as a consequence of:

1) Activation polarizations at the electrodes, representing the energy barriers to charge transfer reactions away from (dynamic) equilibrium at the open circuit potential (OCP).
2) Ohmic resistances to charge transport in the electrolyte, membrane/separator, electrodes and current-collecting plates, together with resistances due to imperfect contacts between layers.
3) Concentration polarizations arising from limitations in the mass transport of reactants to the reaction sites (typically catalyst surfaces).
4) Reactant crossover between electrodes and internal currents

Table 1
Theoretical energy of selected fuels combined with oxygen and hydrogen peroxide at 298 K and 1 atm.

Fuel	Oxidant	Theoretical cell energy charge/ kW h kg^{-1}	References
$NaBH_4$	H_2O_2	17	[70]
$NaBH_4$	O_2	9.3	[102]
Ethanol (C_2H_5OH)	O_2	8.04	[103]
Methanol (CH_3OH)	O_2	6.08	[102]
H_2	O_2	3.28	[104]

Depending on the cell materials, operating conditions and cell chemistry, different losses will dominate. Generally speaking, activation losses dominate at low cell currents, ohmic losses dominate at intermediate currents and concentration losses dominate at high currents, leading to a limiting current value at low cell potentials (associated with a limiting diffusive flux of reactants through a Nernst boundary layer that exists above the reaction surface). Internal currents and fuel crossover losses are apparent from the OCP, which is typically lower than the theoretical reversible value, often appreciably. The cell potential and can be expressed according to the following equation [9]:

$$E_{cell} = E^0_{cell} - |\eta^a_{act}| - |\eta^c_{act}| - |\eta^a_{conc}| - |\eta^c_{conc}| - \sum_k (IR)_k \quad (1)$$

where E_{cell} is the cell potential, E^0_{cell} is the open-circuit potential, η^a_{act} (η^c_{act}) is the activation polarization at the anode (cathode), $(IR)_k$ is the ohmic drop (electronic and ionic) across component k, and η^a_{conc} (η^c_{conc}) is the concentration polarization at the anode (cathode). Fig. 2(a) shows the influence of these losses in a typical polarization curve while Fig. 2(b) shows the physical location of each loss in a parallel plate cell configuration. The anode of a DBFC typically operates at a mixed potential due to the competition between anodic borohydride oxidation and, at the OCP, cathodic water reduction, which is thermodynamically favoured. A mixed potential can also be established at the cathode under low current conditions due to the crossover of borohydride fuel [10,11]. These effects, particularly the mixed anode potential, lead to an OCP that is considerably lower that the theoretical value.

1.2. Sodium borohydride as a fuel

The use of sodium borohydride ($NaBH_4$) in a fuel cell presents many advantages:

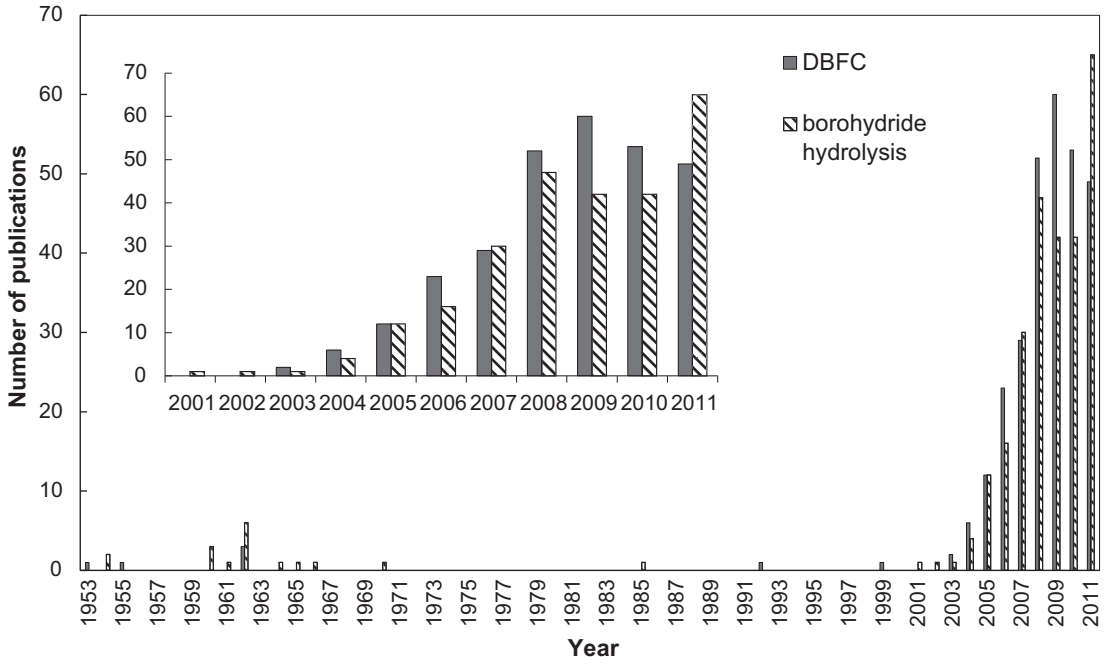

Fig. 1. Evolution of the number of publications related to the direct borohydride fuel cell (DBFC) and the hydrolysis of borohydride [5]. The inset shows a close up between the years 2001 and 2011.

- It is stable in strong alkaline solutions with a half-life of approximately 430 days at pH 14 and is available as a solid or as a 30 wt. % solution [1].
- It contains a large mass concentration of hydrogen (10.6 wt. %) stored in a safe and innocuous form [12].
- It is theoretically able to release $8e^-$ per borohydride ion at a very low electrode potentials (−1.24 V *vs.* SHE) and is able to generate a high power output using a small quantity of fuel [13].
- It does not produce carbon dioxide when used in fuel cells, unlike ethanol or methanol [14], or when used for hydrogen production, unlike hydrocarbons such as natural gas.
- Its oxidation product, metaborate, is environmentally acceptable and can potentially be recycled to sodium borohydride [15].

Table 2
Summary of previous reviews of DBFC.

Year	Author	Tittle	Comments	Ref.
2003	W. Vielstich, A. Lamm, H.A. Gasteiger	Handbook of Fuel Cells—Fundamentals, Technology and Applications	An important review of the science and technology of fuel cells. Little published about DBFC, largely due to a lack of detailed research until 2000	[105]
2003	G. Hoogers	Fuel Cell Technology Handbook	An important review of the science and technology of fuel cells. Little published about DBFC due to lack of research until 2000	[106]
2006	C. Ponce de Leon, F.C. Walsh, D. Pletcher, D.J. Browning, J.B. Lakemanc	Direct borohydride fuel cells	A description of the DBFC, reactions and anode materials tested till date. Influence of electrolyte parameters and comparison. Includes a summary of problems and suggestions for future developments.	[1]
2007	Demirci, U.B.	Direct borohydride fuel cell: Main issues met by the membrane–electrode-assemblies and potential solutions	A review paper focused on the three main issues of the DBFC: namely borohydride hydrolysis and crossover plus the cost of the cell and sodium borohydride production.	[14]
2009	Liu. B. H. L. Z.P.	Current status and progress of direct borohydride fuel cell technology development	A description and comparison of different anode materials and hydrogen evolution on some of them. Brief description of cathode materials and types of electrolyte. Includes a critical summary of cell problems and challenges.	[6]
2009	C. Ponce de Leon, F.C. Walsh	Fuel Cells – Exploratory Fuel Cells : Sodium Borohydride Fuel Cells	An extended review of DBFC and IBFC. Anode materials and mechanism of reactions, electrolyte, temperature conditions and performance of both direct and indirect systems were critically analyzed.	[7]
2010	J. Ma, N.A. Choudhury, Y. Sahai,	A comprehensive review of direct borohydride fuel cells	An extended review of anode and cathode materials. Electrolyte and performance for several experiments carried out on DBFC and stacks, comparison. Includes a summary and challenges.	[8]

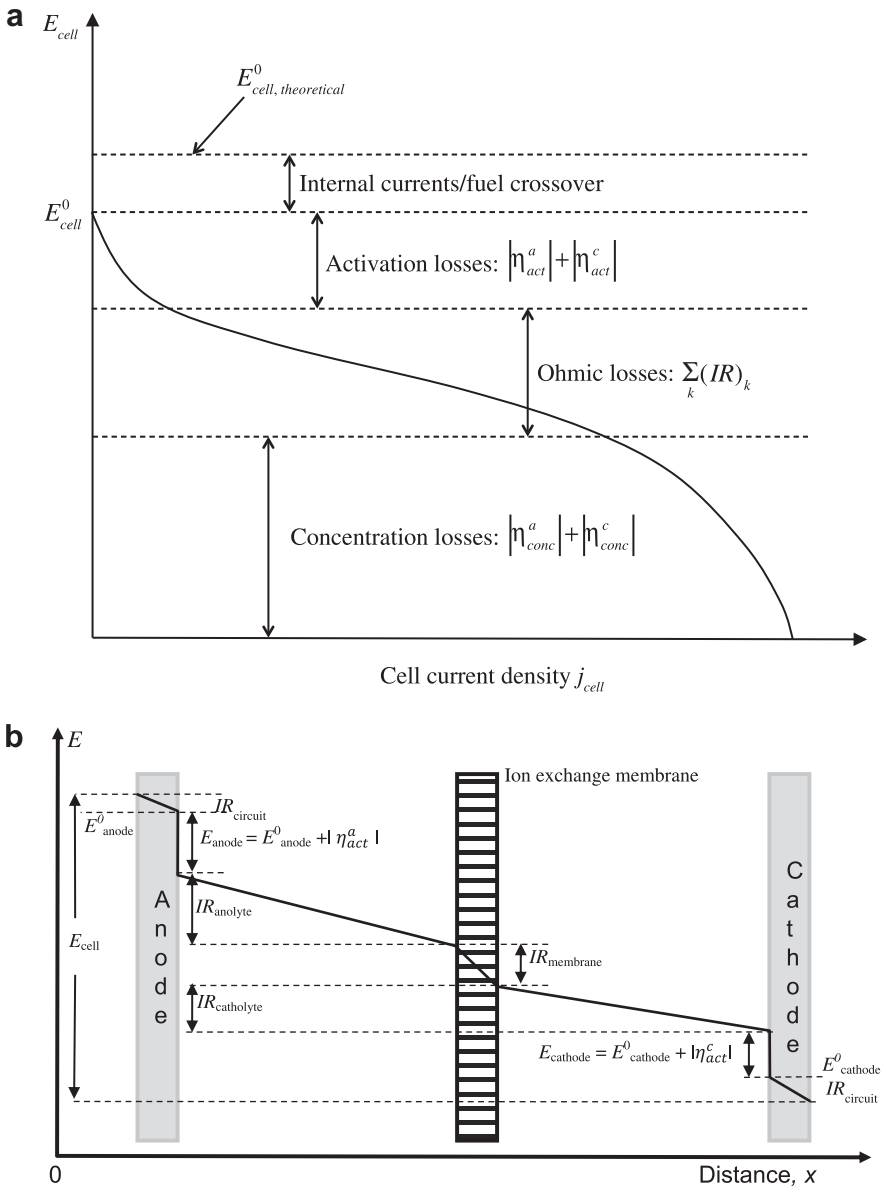

Fig. 2. (a) A parallel-plate electrode, unit cell showing the location of elements that contribute to the overall cell potential drop. (b) The potential across the electrodes, electrolyte and membrane plotted versus the distance between the two parallel electrodes in a divided cell [107].

- It is able to power cells under ambient conditions and the safety of the reactants and products makes it a suitable fuel for portable applications.

Liquid fuels can either store hydrogen, which can be released in a separate reactor to feed a H_2/O_2 fuel cell (as in the IBFC), or the fuel can be oxidised directly at an anode, as in the DBFC; the two cases are illustrated in Fig. 3(a) and (b). The IBFC has already been commercialised with: a guaranteed operation time of 500 h; a continuous output power of 200 W at 10 A current; a stack cell potential of 20–32 V; and a total specific energy of 450–607 W h kg^{-1} [16]. Further research is required to commercialize the DBFC. The best performance documented for a DBFC is a power output of 36 W obtained by Miley et al. using a 25 cm^2 (1.44 W cm^{-2}) $NaBH_4/H_2O_2$ single cell with a Pd/C anode and Au cathode separated by a Nafion 112 membrane [2]. The following sections describe the most important electrocatalysts used in direct borohydride fuel cells.

2. Electrode materials

2.1. Anode

At the anode, the complete oxidation of borohydride ions to release $8e^-$ takes place, in theory, according to the following reaction:

$$BH_4^- + 8OH^- \rightarrow BO_2^- + 6H_2O + 8e^- \quad E^0 = -1.24\text{V vs.SHE} \tag{2}$$

The precise mechanism of borohydride oxidation is still subject to speculation and, therefore, awaits further clarification. The following description represents the current understanding. The initial step is an electron transfer followed by a rapid decomposition of a radical and a further electron transfer step; i.e. an ECE sequence. This oxidation mechanism of BH_4^- is observed in metals with non-catalytic surfaces for hydrogen adsorption, such as Au or Ag, involving an initial electron transfer to form an unstable BH_4^*

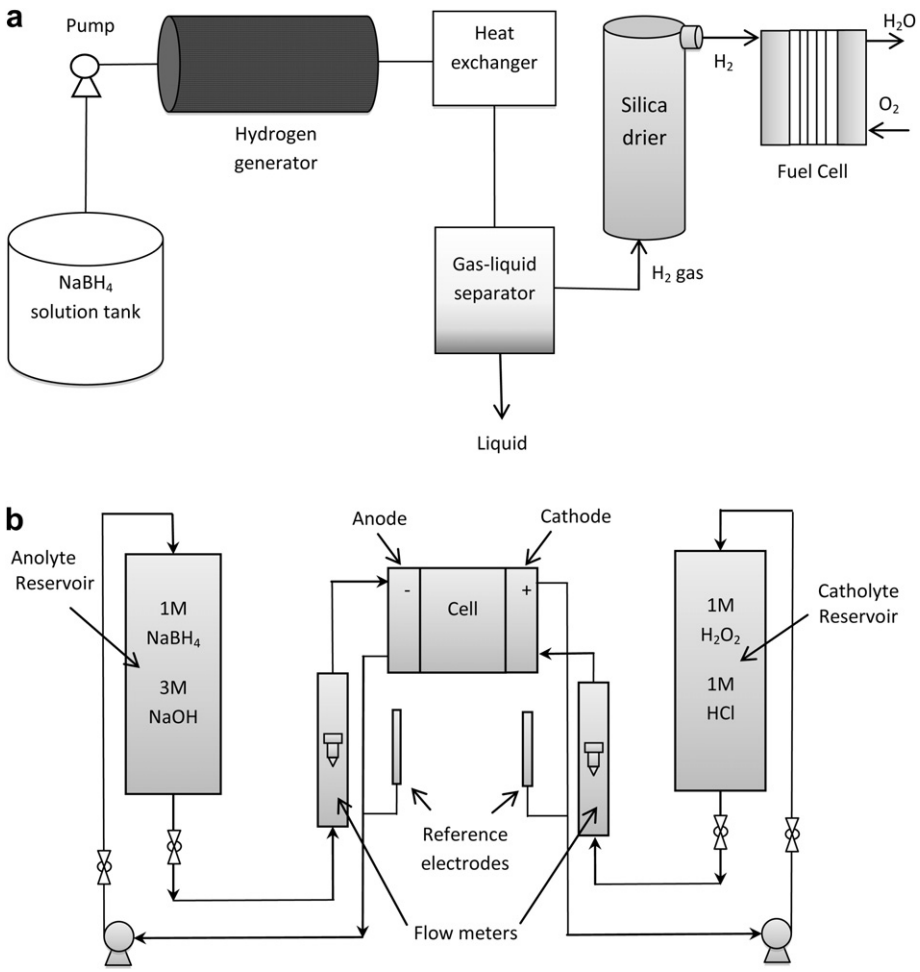

Fig. 3. Typical uses of borohydride solution: a) Hydrogen generation from $NaBH_4$, which is used to fed into a H_2/O_2 fuel cell. The complete arrangement constitutes an indirect borohydride fuel cell (IBFC) system [108]. b) Flow cell system where borohydride is directly oxidised as a fuel. The diagram shows a direct borohydride-hydrogen peroxide fuel cell system [70].

radical. This first step of the mechanism was suggested, on the basis of cyclic voltammetry experiments at 200 V s^{-1} on Au microelectrodes [17]:

$$BH_4^- - e^- \leftrightarrow BH_4^* \quad (E) \tag{3}$$

$$BH_4^* + OH^- \leftrightarrow BH_3^- + H_2O \quad (C) \tag{4}$$

$$BH_3^- + e^- \leftrightarrow BH_3 \quad (E) \tag{5}$$

In the remaining steps of the oxidation, $6e^-$ are thought to be involved in a faster electrochemical reaction, which is still subject to speculation. The reaction mechanism may change depending on the choice of catalyst and reaction conditions, such as the concentration of borohydride or the pH [18]. The actual number of electrons released is typically less than the theoretical 8, due to the parallel unwanted reaction of hydrolysis, which competes with the oxidation:

$$BH_4^- + 2H_2O \rightarrow BO_2^- + 4H_2 \tag{6}$$

This reaction is favoured when (i) the electrolyte is not strongly alkaline, and (ii) in the presence of certain catalysts such as Pt, Ru, Ni, Ni_xB, Co, Co_xB or Pt–$LiCoO_2$ [19]. Considering that reactions (2) and (6) take place at the anode, the electrochemical reaction occurring at the electrode surface can be represented as follows:

$$BH_4^- + xOH^- \rightarrow BO_2^- + 2(x-2)H_2O + (4 - 1/2x)H_2 + xe^- \tag{7}$$

where x is the number of electrons released from each borohydride ion and is also the number of hydroxide ions involved [18]. The competition between BH_4^- direct oxidation reaction and hydrolysis is a function of the electrode material, the electrolyte composition and the electrode potential [2]. It has been demonstrated that for a ratio of OH^- to BH_4^- concentrations of approximately 4.4, the oxidation releases 8 electrons, while for lower ratios the concentration of protons increases, lowering the pH and increasing the concentration of intermediate species (BH_3OH^-), which leads to a decrease in the number of electrons liberated [20].

The mechanism of reaction (7) is likely to involve an initial pre-disassociation step at the active surface sites, for example, at a platinum electrode [21,22]:

$$BH_4^- + Pt \leftrightarrow Pt - BH_3 + H^+ + 2e^- \tag{8}$$

This step could be followed by the adsorption of hydrogen ions on the metallic surface, particularly in metals M that are able to promote the pre-dissociation step, such as Pt, Pd or Ni [1]:

$$2M + BH_4^- \rightarrow M - H + M - BH_3^- \tag{9}$$

This reaction is followed by an electron transfer step (E), a further chemical surface reaction (C) and the combination of

hydrogen atoms producing hydrogen gas [18]. The oxidation of borohydride ions at Pt electrodes is complicated by the catalytic hydrolysis and oxidation of the intermediates. The CE mechanism of BH_4^- at Pt follows the sequence below [13]:

$$BH_4^- + H_2O \rightarrow BH_3OH^- + H_2 \quad (C) \tag{10}$$

$$H_2 + 2OH^- \rightarrow 2H_2O + 2e^- \quad (E) \tag{11}$$

$$BH_3OH^- + 3OH^- \rightarrow BO_2^- + \frac{3}{2}H_2 + 2H_2O + 3e^- \quad (E) \tag{12}$$

The intermediate product of the borohydride oxidation (BH_3OH^- ions) can either be oxidised (at more negative potentials) or hydrolysed, and the number of electrons obtained from one molecule of borohydride can vary depending on which route is taken. The electron-transfer reaction rate during borate ion (BO_2^-) formation (reaction (12)) varies with the nature of the electrode material - whether or not it catalyzes the hydrogen evolution reaction (10). In most studies, the BH_3OH^- ion was proposed as an intermediate during oxidation at Pt, Pd, Au, or Hg anodes. This intermediate was considered to be bound to Pt or Au surfaces [23]. Gyenge [20] has proposed that the oxidation pathways taken may depend on the surface adsorption of both BH_4^- and various reaction intermediates. The irreversibility of the borohydride oxidation is the result of very unstable intermediates such as the short-lived radical BH_4^* [3]. Fig. 4 shows a general overview of the different pathways that the borohydride oxidation reaction can follow depending on the catalyst and the concentration of hydroxide ions.

Studies have been conducted on a wide range of anode catalysts in order to assess their effect on borohydride oxidation and cell performance [2,6,11,18,20,24–26]. Electrode materials active towards borohydride hydrolysis include Pt, Ru, Ni, Ni_xB, Co, Co_xB, Pt–$LiCoO_2$, whereas non-active materials for hydrolysis are Hg, Au, and possibly Ag [19]. Non-precious materials such as Ni and Cu have also been investigated as catalysts for the anodic reaction in DBFCs [18]. Few studies have taken into account the cathode catalyst and its influence on fuel cell performance [23,25,27–29], which is somewhat surprising considering that the cathode is often found to be limiting [30–32].

Fig. 5 shows a comparison of the power density obtained from a BH_4^-/O_2 DBFC of 4 cm^2 active geometric area with different anode materials. In all cases, the cathode was Pt/C (2 mg Pt cm^{-2}), a Nafion 117 membrane was used to separate the anode and cathode compartments, and the operating temperature was 85 °C with an electrolyte containing 5 wt. % (1.32 mol dm^{-3}) $NaBH_4$ in 10 wt. % (2.5 mol dm^{-3}) NaOH [33,34]. The highest peak power density of 89.6 mW cm^{-2} was obtained using Pd/C as the anode catalyst, followed by Au/Ti (around 80 mW cm^{-2}) and Au/C (72.2 mW cm^{-2}). The lowest peak power density was 40.5 mW cm^{-2}, obtained with a Ni/C catalyst. When a Zr–Ni laves-phase alloy was used as the anode catalyst, with a solution containing 10 wt. % (2.64 mol dm^{-3}) $NaBH_4$ in 20 wt. % (5 mol dm^{-3}) NaOH fed to the anode compartment [30], the peak power density of the cell increased to around 190 mW cm^{-2}.

2.1.1. Platinum and its alloys

The number of electrons transferred during the oxidation of borohydride ions at a Pt electrode lies between 2 and 4 [3], depending on the concentration of borohydride ions [19,35]. The heterogeneous rate constant obtained for the four-electron transfer during the direct oxidation of BH_4^- at Pt is ten-fold that for the eight-electron oxidation on Au [20]. The reactions of oxidation or hydrolysis of borohydride on these metals must produce the

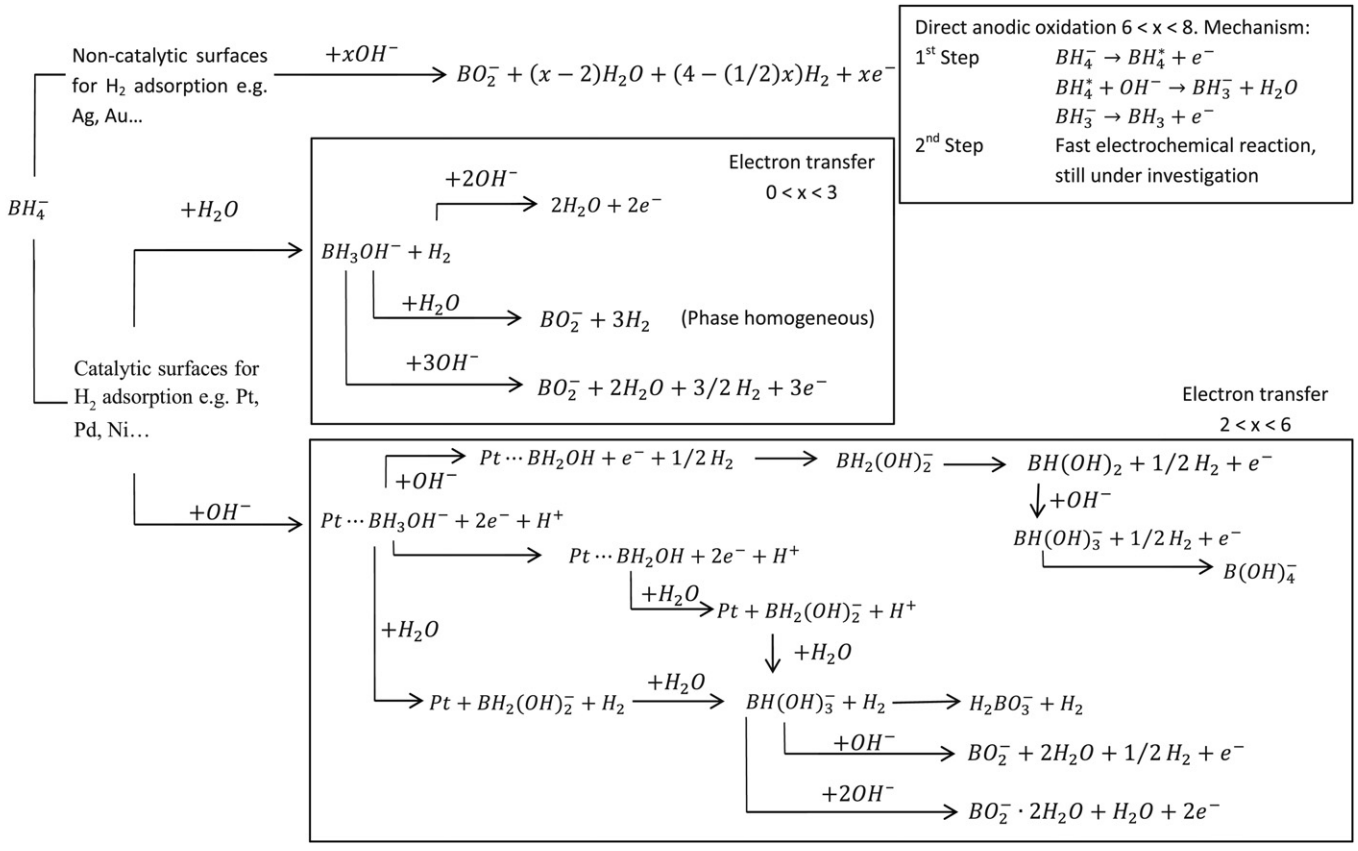

Fig. 4. Reaction pathways involving anodic oxidation of borohydride ion and competitive reactions [22,109].

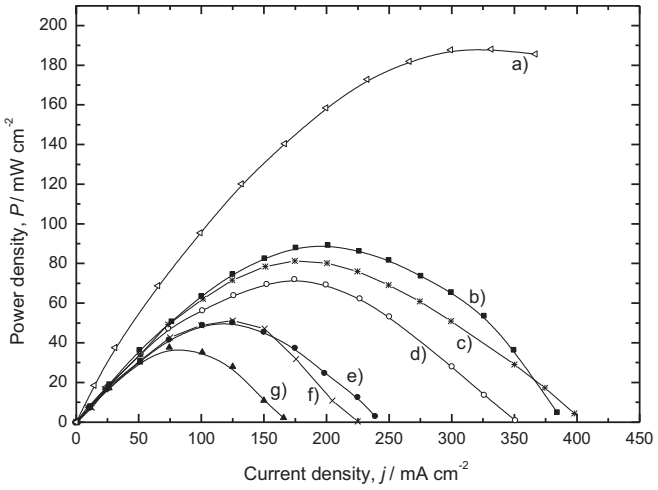

Fig. 5. Power densities (P) *vs.* current density in a BH_4^-/O_2 DBFC with different anodes of 4 cm^2 active area: a) $Zr_{0.9}Ti_{0.1}Mn_{0.6}V_{0.2}Co_{0.1}Ni_{1.1}$, b) Pd/C, c) Au/Ti, d) Au/C, e) Ag/Ti, f) Pt/C, g) Ni/C. Cathode: Pt/C (2 mg Pt cm^{-2}). Membrane: Nafion 117. Temperature: 85 °C. Fuel: a): 10 wt. % (2.64 mol dm^{-3}) $NaBH_4$ in 20 wt. % (5 mol dm^{-3}) NaOH [30]; b)-g): 5 wt. % (1.32 mol dm^{-3}) $NaBH_4$ in 10 wt. % (2.5 mol dm^{-3}) NaOH [33,34].

breaking of four B–H bonds. Density functional theory (DFT) calculations suggest that these bond breaking reactions are slower on gold than on platinum surfaces, indicating a higher overpotential for BH_4^- oxidation at Au surfaces [36].

Several binary Pt alloys have been tested, including Pt-Ir, Pt-Ni, Pt-Au, Pt-Ru/C and Ag–Pt [19]. Gyenge et al. [19] synthesised and investigated a bimetallic Pt–Au catalyst that could theoretically combine the favourable kinetics on Pt with the higher coulombic efficiency for borohydride oxidation on Au. Experiments with a DBFC were carried out using a 2 mol dm^{-3} $NaBH_4$ in 2 mol dm^{-3} NaOH solution on the anode side, a 5 mg cm^{-2} colloidal anode loading, a Nafion 117 membrane, and an O_2 gas diffusion cathode containing 4 mg cm^{-2} Pt. The results obtained showed that the peak current was higher, and that the oxidation peak potentials were shifted to more negative values on Pt–Au compared to pure Pt. The number of electrons transferred during the borohydride ion oxidation was 8 on the Pt–Au alloy. Pt–Ir and Pt–Ni were also tested as working electrode catalysts for the same cell. The results showed that Pt–Ir and Pt–Ni were the most active anode catalysts, giving (in both cases) a power density of 53 mW cm^{-2} at 75 °C. Pt–Ir showed potentially favourable kinetics, with the oxidation peaks shifted to more negative potentials than those observed with Pt–Ni, and yielding the highest voltammetric BH_4^- oxidation current densities at potentials more negative than −0.4 V *vs.* MMO (mercury/mercury oxide reference electrode), which is ultimately the domain of interest for borohydride fuel cells. Both, Pt–Ir and Pt–Ni gave the highest cell potentials at any given current density, e.g., at 100 mA cm^{-2} and 333 k the cell potential was 0.53 V *vs.* MMO with an anode catalyst loading of 5 mg cm^{-2} in the anode.

Duteanu et al. [11] reported experiments using a binary alloy of Pt and Ru deposited on a carbon anode together with a Pt/C cathode in a MEA. The catalyst loading was 1 mg cm^{-2} in both cases. The cell gave power densities of 145 and 110 mW cm^{-2} using oxygen and air cathodes, respectively, with a cathode flow rate of 0.4 cm^3 min^{-1} at 60 °C and borohydride concentrations of 1 mol dm^{-3} in sodium hydroxide 1 mol dm^{-3}. Concha et al. [37] suggested that the combination of Ag and Pt could improve the cell performance since Ag promotes the direct oxidation of borohydride, whereas Pt helps to increase the reaction rate. The authors tested the Ag–Pt alloy as an anode catalyst for borohydride oxidation using 0.001 mol dm^{-3} $NaBH_4$ in 0.1 mol dm^{-3} NaOH at 25 °C. The borohydride oxidation reaction was faster on Pt than on Ag, the measured current density being 0.02 A cm^{-2} for the former and 1.4×10^{-7} A cm^{-2} for the latter at 0.65 V *vs.* SHE [37]. Two different compositions of Pt–Ag alloy were prepared, PtAg composed of 94.5% Pt and AgPt with 8.4% Pt. The number of electrons transferred on both alloys at the limiting current was 4 and it was concluded that Ag in PtAg favours the direct pathway to the oxidation of borohydride ions, while Pt in AgPt enhances the borohydride oxidation reaction kinetics. As a result, both Pt–Ag alloys show a unique and comparable behaviour with respect to borohydride oxidation: unlike Pt alone, they do not catalyse the quantitative heterogeneous hydrolysis of BH_4^- followed by the hydrogen oxidation reaction but instead drive the borohydride oxidation reaction towards the direct pathway.

2.1.2. Gold

A number of investigations have been carried out with different stationary and rotating electrodes based on gold, and good performance for borohydride oxidation has been observed [13,24]. The experiments demonstrate that 8 electrons are released during the direct oxidation, which suggests that hydrolysis does not occur during operation [17,25,38]. Recent findings, however, contradict this conclusion. Chatenet et al. [39] claimed that the amount of hydrogen released at a Au electrode is not negligible and they proposed that the borohydride oxidation pathway can be different at low ($E < 0.3$–0.5 V *vs.* RHE) and high potential values ($E > 0.3$–0.5 V *vs.* RHE). They pointed out that if the hydrolysis of borohydride ions proceeds in two steps (reactions (13) and (14)) and the first step of the mechanism of reaction of borohydride oxidation is as shown in reaction (15) [17], then BH_3OH^- can be produced through either reaction (13) or reaction (15).

$$BH_4^- + H_2O \rightarrow BH_3OH^- + H_2 \quad (13)$$

$$BH_3OH^- + H_2O \rightarrow BO_2^- + 3H_2 \quad (14)$$

$$BH_4^- + 2OH^- \rightarrow BH_3OH^- + H_2O + 2e^- \quad (15)$$

Chatenet et al. [39] suggest that, at low overpotentials, the oxidation of BH_3OH^- on gold can involve three electrons; reaction (13) followed by reaction (16) to six electrons; reaction (13) followed by reaction (17):

$$BH_3OH^- + 3OH^- \rightarrow BO_2^- + 1.5H_2 + 2H_2O + 3e^- \quad (16)$$

$$BH_3OH^- + 6OH^- \rightarrow BO_2^- + 5H_2O + 6e^- \quad (17)$$

At high overpotentials, the activity of Au for the oxidation of BH_3OH^- is important and the direct oxidation of borohydride, reaction (15), occurs, followed by the oxidation of the intermediate (BH_3OH^-), reaction (16) or (17), releasing between five and eight electrons in total. It is also possible that an overall EC mechanism takes place, where BH_3OH^- is formed through reaction (15) then hydrolysed through reaction (14), in which case more hydrogen will be generated. Finkelstein et al. [13] suggested that Pt can outperform Au for DBFCs, providing similar charge efficiency at less positive anode potentials. They did not, however, consider the hydrolysis problem on Pt.

2.1.3. Silver

According to Concha et al. [35] the number of electrons released on Ag varies from 2 at pH 12.6 to 6 at pH 13.9 (at 25 °C). Ag, however, exhibits slow electrode kinetics and low power densities [6]. Atwan et al. [40] suggested that alloying Ag with Ir and Pt could effectively improve the electrode kinetics. It is also necessary to take into account the presence of oxides on the Ag surface. Studies

related to the formation of oxides on Ag electrodes in alkaline media [41,42] show that Ag oxide layers were formed and present during borohydride oxidation [41]. Sanli et al. [42] have also shown that oxides formed on the Ag surface by cyclic voltammetry have a catalytic effect on the oxidation of borohydride. The oxidation of borohydride appears to be promoted at high pH due to the formation of a multi-layered oxide film (Ag_2O) on the catalyst surface. They found that the number of electrons transferred on silver oxide was 6 and suggested the following anodic reaction:

$$Ag_2O + BH_4^- + 6OH^- \rightarrow 2Ag + BO_2^- + 5H_2O + 6e^- \quad (18)$$

2.1.4. Nickel

Borohydride ions are very active even at non-precious metals such as Ni. The consensus is that the oxidation of borohydride ions on Ni involves the transfer of 4 electrons (the other 4 electrons are possibly lost in the formation of hydrogen gas), although high current densities can be reached at an acceptable potential (e.g. 300 mA cm^{-2} at −0.7 V *vs.* SHE) [1]. Liu et al. [18] experimented with Ni, Raney Ni, Pd, Pt, Cu and Au as anode catalysts in order to compare their OCPs. They used a solution containing 6 mol dm^{-3} $NaBH_4$ in 6 mol dm^{-3} NaOH, and a Nafion membrane in the MEA. Under the same conditions, Ni and Ni Raney electrodes exhibited the most negative OCPs of −1.03 V *vs.* SHE, followed by Cu and Au with values of −1.02 and −0.99 V *vs.* SHE, respectively, and Pt and Pd with values of −0.91 V *vs.* SHE [18]. The highest efficiencies, on the other hand, were achieved with Pd and Pt electrodes under certain conditions, such as a relatively low borohydride concentration and/or a large anodic current [6,19]. Liu et al. [43] reported the polarization curves in a cell with a Ni anode catalyst and a metal hydride as the cathode catalyst, together with a Nafion membrane to separate the two electrodes. The results showed values of 200 mA cm^{-2} at −0.7 V *vs.* Hg/HgO using a solution of 1.6 wt. % KBH_4 (0.4 mol dm^{-3}) in 6 mol dm^{-3} KOH at 20 °C. Suda et al. [30] reported a cell potential of 0.6 V at 150 mA cm^{-2}, operating at 60 °C, when they used a Zr–Ni laves phase alloy as an anode catalyst at a loading of 200 mg cm^{-2}. Ma et al. [44] investigated Ni compositae anodes, such as Ni + Pt/C and Ni + Pd/C (the ratio of Pt–Ni or Pd–Ni was 25:1). A borohydride-oxygen fuel cell consisting of 1 mg cm^{-2} Pt/C cathode separated from the anode by a Nafion membrane was assembled. The anolyte was 5 wt. % $NaBH_4$ (1.32 mol dm^{-3}) in 10 wt. % (2.5 mol dm^{-3}) NaOH aqueous solution, flowing at a rate of 5 cm^3 min^{-1}. The cell was operated for 100 h to monitor its performance and stability. When carbon-supported palladium or nickel powders (10% on Vulcan XC-72 carbon) were used on a carbon cloth surface the power density was 33 mW cm^{-2} lower than that obtained using Pt–Ni/C under similar conditions, which reached a value of 237 mW cm^{-2}. A higher power density, up to 665 mW cm^{-2} (at 60 °C and with 1 mg Pt–Ni cm^{-2} loading and a Pd/C cathode 1 mg cm^{-2}) was achieved in a $NaBH_4/H_2O_2$ system [44].

2.1.5. Zinc

Zn could be an appropriate anode catalyst for the DBFC since, in theory, it is a relatively poor electrocatalyst for hydrogen adsorption and reduction, it is a low cost material and it is suitable for energy storage [45]. Santos and Sequeira [45] performed experiments using a Zn disk of 0.5 cm^2 surface area, a Pt mesh as a counter electrode and a solution containing 1 mol dm^{-3} $NaBH_4$ in 4 mol dm^{-3} NaOH as the anolyte. A volumetric mixture ratio of 1:2:5 H_2O_2 in 1 mol dm^{-3} HCl was used as the catholyte. A Nafion 117 membrane was used to separate the anode and cathode compartments. An electrode potential of −1.57 V *vs.* SCE was obtained, which, according to the Pourbaix diagram [46], could correspond to the reaction:

$$ZnO_2^{2-} + 4H^+ + 2e^- \rightarrow Zn + 2H_2O \quad (19)$$

The potential value was more negative than that obtained with other metals and offers the possibility of achieving a higher cell potential. Cyclic voltammetry showed an oxidation peak corresponding to borohydride ion oxidation at −1.16 V *vs.* SCE, reaching a current density of 200 mA cm^{-2}. At more positive potential values, a layer of Zn oxide (covering the electrode surface) was formed, which inhibited borohydride oxidation. During the reverse potential scan, reduction of this layer occurred and the anode surface was reactivated allowing borohydride and/or its intermediates products to be oxidised. It was found that four electrons were transferred during the oxidation of borohydride ions at this electrode. However, hydrogen evolution at the Zn surface only takes place for very negative potentials (<−1.9 V *vs.* SCE). A reaction mechanism proposed by Santos and Sequeira [45] consists of reaction (19) followed by:

$$BH_4^- + 2OH^- \rightarrow BH_3OH^- + H_2O + 2e^- \quad (20)$$

The BH_4^-/H_2O_2 cell potential obtained by Santos and Sequeira [45] was 2.14 V, which is appreciably lower than the theoretical value (3 V) for BH_4^-/H_2O_2 system. A stability test showed that the cell was able to operate for short periods of time (no more than 6 h), depending on the ohmic losses within the cell, which increase linearly as the current rises. Below cell potentials of 1.4 V, the discharge current dropped dramatically. The cell discharge curves showed a power density of 528 mW cm^{-2} for 0.8 s, a specific capacity of 1577 A h kg^{-1} and an energy density as high as 2799 W h kg^{-1}. Polarization data showed anode limitations during short-time operation, particularly at high cell currents [45].

2.1.6. Palladium

Palladium is catalytically active towards both the electrochemical oxidation of borohydride and its hydrolysis, yielding large anodic currents and high charge efficiencies at relatively low borohydride concentrations. The oxidation on palladium/carbon electrodes involves six electrons with 75% efficiency as shown in the following reaction [18,43]:

$$BH_4^- + 6OH^- \rightarrow BO_2^- + 4H_2O + H_2 + 6e^- \quad (21)$$

Liu et al. [18], however, suggested that when a higher concentration of BH_4^- is used, the reaction can involve 4 electrons. Celik et al. [47] carried out experiments in a direct borohydride flow cell using a an MEA with a Pd/C anode and a Pt/C cathode divided by a Nafion membrane. A maximum power density of 27.6 mW cm^{-2} at a cell potential of 0.85 V was obtained with a single cell of 25 cm^2 active electrode area operating at 60 °C, with 1 mol dm^{-3} $NaBH_4$ in 20 wt. % (5 mol dm^{-3}) NaOH. The highest power was obtained when the highest anode catalyst loading was used, increasing by 34% when the loading increased from 0.3 to 1.08 mg cm^{-2} Pd/C. Miley et al. [2] used an MEA arrangement consisting of Pd/C anode, Au/C cathode and a Nafion 112 cationic exchange membrane to construct a 500 W cell–stack of 15 $NaBH_4/H_2O_2$ fuel cells with an active area of 144 cm^2 per cell, resulting in a power density of 231 mW cm^{-2}.

2.1.7. Osmium and copper

Atwan et al. [26] reported cyclic voltammetry experiments on finely-divided Os particles supported on Vulcan carbon powder and Os-alloys (OS–Sn, Os–Mo and Os–V) for the direct oxidation of borohydride ions. A three-electrode cell with a graphite rod counter electrode was used. Using a solution containing 0.03 mol dm^{-3} of $NaBH_4$ in 2 mol dm^{-3} NaOH the oxidation potentials were between 0.1 V and 0.3 V *vs.* Ag/AgCl, KCl_{std} with a peak current density of

40 mA cm^{-2} for Os and values of around 40, 20 and 10 mA cm^{-2} for Os–Mo, Os–Sn and Os–V, respectively. It was also argued that the operating potentials of colloidal Os-alloys are more positive than those of Os colloids; therefore, alloying Os with Mo, Sn or V does not have any benefit. In conclusion, borohydride ion oxidation was observed on colloidal Os and Os-alloys but low current densities were obtained.

Using a three-electrode DBFC with a Cu anode, a Pt cathode and an NRE212 membrane, operating at room temperature containing an anolyte of 2 mol dm^{-3} $NaBH_4$ in 2 mol dm^{-3} NaOH, Zhi-fang et al. [48] obtained a maximum current density and a maximum power density of 235 mA cm^{-2} and 46.14 mW cm^{-2}, respectively. A stable cell potential of around 0.6 V was obtained for 50 h at a current density of 20 mA cm^{-2}.

2.1.8. Other catalyst materials

AB_5 and AB_2-type hydrogen storage alloys have also been identified as appropriate anode catalysts for DBFC [49,50]. These metallic materials have the ability to absorb and release significant amounts of hydrogen gas. In the AB_5 alloys, A is an hydride forming metal, usually a rare earth metal (e.g., La, Ce, Nd, Pr, Y or a mixture (mischmetal)) and B is a non-hydride forming element, such as Ni, which can be doped with other metals (e.g., Co, Sn or Al) to improve the stability or to adjust the equilibrium hydrogen pressure and temperature required to charge/discharge hydrogen [50]. In the AB_2 alloys, A represents a large group of alloys containing Ti, Zr or Hf, and B represents a transition metal (e.g., Mn, Ni, Cr or V). Higher power densities are achieved with the AB_5-type alloys [31], probably due to their higher capacities at high discharge rates [51].

Hydrogen storage alloys are expected to mitigate hydrogen evolution in DBFCs since they can absorb large quantities of hydrogen gas. Wang et al. [51] reported that the $L_mNi_{4.78}Mn_{0.22}$ (where Lm is a La-rich mischmetal) hydrogen storage alloy exhibits a high electrochemical catalytic activity towards both hydrogen generation and the oxidation of borohydride. Although this appears to lead to an inefficient anode material the authors suggest that an electrochemical surface treatment of the alloy can help to decrease the hydrogen evolution. The alloy was modified by the addition of Si followed by heat treatment and used as an anode catalyst in a DBFC. These modifications decreased the rate of hydrogen generation, resulting in more than four-fold increase in the fuel utilization efficiency (from 21.4% to 95.3%). The electrochemical catalytic activity of the anode, however, was appreciably lower [52].

Various AB_5- and AB_2-type hydrogen storage alloys have been employed as anode catalysts in DBFCs [53–58]. Lee et al. [21] reported that the use of $ZrCr_{0.8}Ni_{1.2}$ (an AB_2-type alloy) led to hydrogen generation from the borohydride through a stepwise mechanism, followed by the electrochemical oxidation of hydrogen to further liberate electrons. Choudhury et al. [31] reported a power density of 150 mW cm^{-2} at a cell potential of 0.54 V while operating at 70 °C using $M_mNi_{3.55}Al_{0.3}Mn_{0.4}Co_{0.75}$ (5 mg cm^{-2}) as the anode catalyst and 60 wt. % Pt on carbon as the cathode catalyst, with a platinum loading of 1 mg cm^{-2}. A solution containing 10 wt. % (2.64 mol dm^{-3}) $NaBH_4$ in 20 wt. % (5 mol dm^{-3}) NaOH was used. Li et al. [59] obtained a higher power density (290 mW cm^{-2}) with a five-cell stack of 67 cm^2 active area. A power of 110 W was achieved starting at room temperature and reaching 60 °C during operation. The cell consisted of a Pt/C air cathode, a Nafion

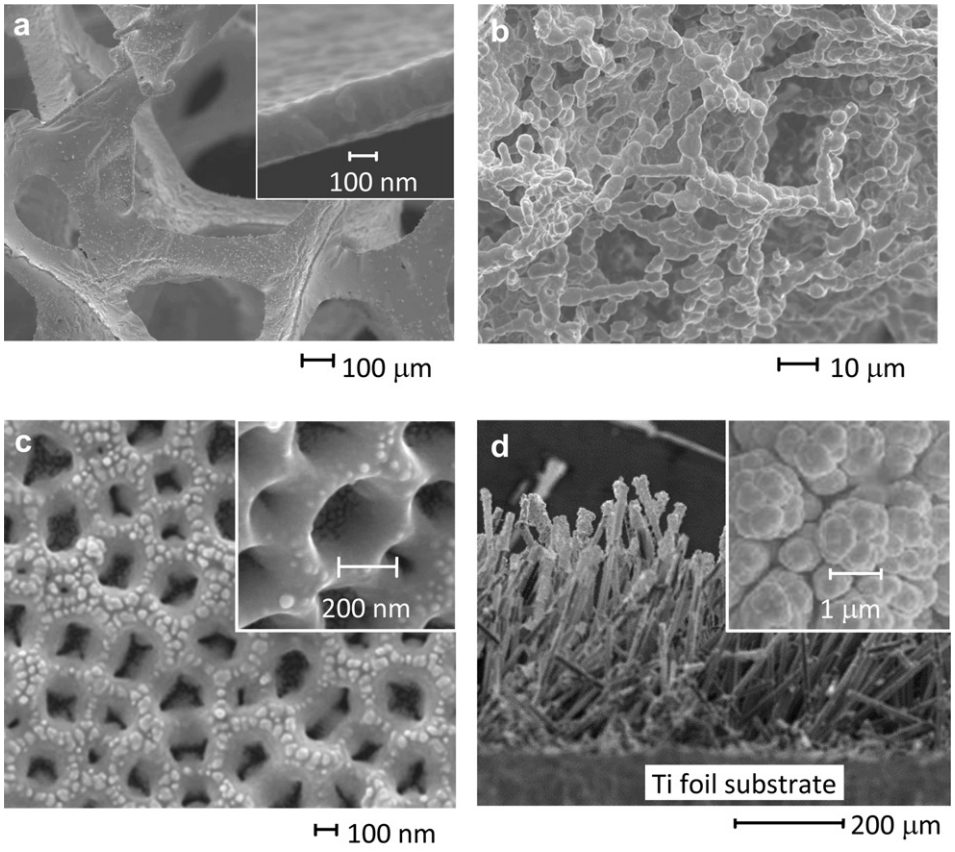

Fig. 6. SEM images of four different three-dimensional electrodes used for the oxidation of borohydride ions: a) Gold-coated RVC 80 ppi prepared by sputtering technique, the inset shows the thickness of the deposit on the carbon substrate [64], b) Silver sponge porous electrode prepared by calcination of a mixture of $AgNO_3$ and dextran [64], c) gold coated titanium nanotubes produced by anodisation [65], d) Carbon fibres deposited by direct charging electrostatic flocking (DCEF) [66]. The authors are grateful to Dr J. Low from the University of Southampton and Dr C. Patrissi from the Naval Undersea Warfare Centre for the images c) and d) respectively.

membrane (NRE-211) and a mixture of surface treated Zr–Ni Laves phase alloy AB_2 ($Zr_{0.9}Ti_{0.1}Mn_{0.6}V_{0.2}Co_{0.1}Ni_{1.1}$) and Pd/C as the anode catalyst. Other materials such as Ru or Co have been reported to act as good catalysts for borohydride hydrolysis, rendering them appropriate for an IBFC rather than a DBFC [60,61].

2.1.9. Three-dimensional electrodes

The space-time yield and space velocity in electrochemical reactors containing two-dimensional electrodes can be increased using three-dimensional electrodes such as reticulated vitreous carbon (RVC), reticulated nickel (RN) or a silver sponge [62]. The high surface area and high porosity of these electrodes render them ideal as fuel cells electrode substrates, since high rates of conversion per unit volume can be achieved [63]. Ponce de León et al. [64] investigated the use of three-dimensional electrode supports (such as RVC) of different porosity grades coated with gold nanoparticles, as well as a silver porous sponge. The current generated by the oxidation of borohydride ions and the values of the heterogeneous oxidation rate constants tended to increase with the porosity grade of the electrode and the deposition time of the gold nanoparticles. Silver sponge electrodes prepared from the calcination of a polymer matrix and silver nitrate mixtures showed reasonable activity towards the oxidation of borohydride ions at positive potentials. Fig. 6 shows four different three-dimensional electrodes used in the borohydride system. In Fig. 6(a) a gold-coated RVC 80 ppi prepared by the sputtering technique is displayed [64]. The inset in Fig. 6(a) shows that the thickness of the gold deposit was approximately 200 nm thick and firmly attached to the RVC substrate. Other 3D electrodes used for borohydride oxidation were a silver porous sponge prepared by calcination of a mixture of silver nitrate and dextran (shown in Fig. 6(b)) [64], and gold-coated titanium nanotubes prepared by anodising a titanium plate (shown in Fig. 6(c)) [65]. Fig. 6(d) shows a carbon fibre electrode manufactured by direct charging electrostatic flocking (DCEF) and coated with a Pd/Ir alloy. This electrode was used as a cathode in a direct borohydride-hydrogen peroxide fuel cell [66].

Fig. 7 compares the forward scans from cyclic voltammograms of two- and three-dimensional electrodes during the oxidation of borohydride. This figure shows that the peak oxidation potentials of borohydride on the three-dimensional electrodes, gold coated RVC (curve a) and silver sponge (curve b), occurs at 0.0 V *vs.* SCE and at −0.16 V *vs.* SCE, respectively. The oxidation on a two-dimensional electrode gold plate (curve c) occurs at a more negative value of −0.6 V *vs.* SCE. The shift towards positive potentials in the three-dimensional electrodes is probably due to the IR drop commonly observed in porous structures. Furthermore, activation overpotentials between 200 and 300 mV higher can be observed on the three-dimensional electrodes in comparison with the two-dimensional electrode. This represents higher energy barriers to borohydride oxidation, which, nevertheless, are compensated by the higher current density (per geometric area) provided by the three-dimensional structure. The silver porous electrode shows a higher current than a gold-coated RVC (10 ppi) of approximately similar size and the two-dimensional gold electrode plate of 3 cm^2.

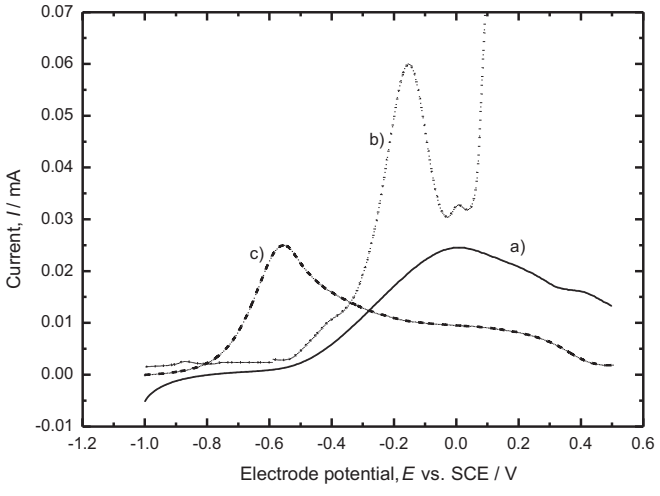

Fig. 7. Cyclic voltammograms of 0.02 mol dm^{-3} $NaBH_4$ in 3 mol dm^{-3} NaOH on different types of electrodes: a) 10 ppi RVC gold-coated by sputtering technique for 1 min, b) Silver sponge porous electrode and, c) gold plate electrode of 3 cm^2 area. The dimensions of the 3D electrodes were approximately 1 cm × 0.5 cm × 0.5 cm and the potential sweep rate for all the electrodes was 20 mV s^{-1} at 298 K.

2.2. Cathodic reaction

Two oxidizers have been used extensively for the cathodic reaction in DBFCs: O_2 and H_2O_2. Hydrogen peroxide is a good alternative for anaerobic applications, namely, underwater vehicles and space [1,2]. The reduction of H_2O_2 is a faster process than that of oxygen, which enhances the power density and the cell efficiency [23]. The reduction mechanism depends on the electrolyte medium and can occur at different electrode potentials:

1 Oxidant: O_2 Alkaline electrolyte

$$2O_2 + 4H_2O + 8e^- \rightarrow 8OH^- \quad E^0 = 0.4\ \text{V } vs.\ \text{SHE} \tag{22}$$

2 Oxidant: H_2O_2 Alkaline electrolyte

$$4HO_2^- + 4H_2O + 8e^- \rightarrow 12OH^- \quad E^0 = 0.87\ \text{V } vs.\ \text{SHE} \tag{23}$$

3 Oxidant: H_2O_2 Acid electrolyte

$$4H_2O_2 + 8e^- + 8H+ \rightarrow 8H_2O \quad E^0 = 1.77\ \text{V } vs.\ \text{SHE} \tag{24}$$

$NaBH_4/H_2O_2$ fuel cells exhibit higher cell potentials in acidic media ($E_{cell} \cong 3$ V) which represents a predicted energy density of 17,060 W h kg^{-1}, as is shown in Table 1 [4]. From the operational point of view, the fact that all the components are liquids presents advantages in terms of storage, pumping requirements and heat removal.

2.2.1. Cathode materials

The preceding discussion highlights the vast effort directed at finding suitable anode catalysts for DBFCs. In contrast, the choice of cathode catalyst has been rather limited; most investigators have used Pt. Alternatives, such as Pt/C, Au/C, Ag/C, MnO_x/C and MnO_x-Mg/C, were investigated by Chatenet et al. [25]. The authors suggested that Pt/C, Ag/C and Au/C should not be used as DBFC cathode catalysts, since they exhibit electrocatalytic activity towards BH_4^- oxidation (which takes place due to crossover, particularly at low currents/near the OCP). This reaction competes for the active sites on the catalyst surface, leading to deterioration in the cell performance. Chatenet et al. maintain, however, that MnO_x/C and MnO_x-Mg/C are unaffected by the presence of borohydride and are, therefore, appropriate as cathode catalysts in BH_4^-/O_2 fuel cells.

In BH_4^-/H_2O_2 fuel cells, Pt, Au, Pd, Ag, Raney Ag, Pd/Ir, Pd–Ru, and Pd–Ag have been studied as cathode catalysts for H_2O_2 reduction [25,27,28,67]. A good cathode catalyst material will reduce the hydrogen peroxide to produce water and will not decompose it to produce oxygen according to the following reaction [23]:

$$2H_2O_2 \rightarrow O_2 + 2H_2O \tag{25}$$

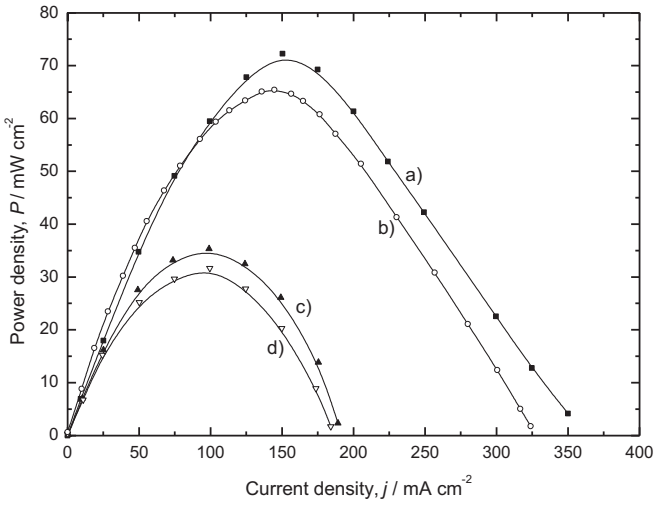

Fig. 8. Power densities (P) *vs.* current density curves measured in a BH_4^-/O_2 fuel cell using Au/C anode of 4 cm^2 active area (2 mg Au cm^{-2}) and cathodes (2 mg material cm^{-2}): a) Pt/C, b) FeTMPP, c) Ni/C, d) Ag/C. Membrane: Nafion 117. Temperature: 85 °C. Fuel: 5 wt. % (1.32 mol dm^{-3}) $NaBH_4$ in 10 wt. % (2.5 mol dm^{-3}) NaOH [33,68].

Pt in the cathode typically yields excellent performance in terms of power density; however, it tends to decompose peroxide rapidly [2]. Both Au and Pd based cathode catalysts have exhibited good performance [23,29], minimizing oxygen evolution from the hydrogen peroxide decomposition and providing high power densities. A peak power density of 680 mW cm^{-2} at 60 °C was achieved in a BH_4^-/H_2O_2 fuel cell with a Pd anode catalyst, prepared by applying a 1:1:20 mixture of Nafion-Pd-methanol on a carbon cloth diffusion layer, combined with an Au cathode catalyst (0.5 mg cm^{-2}) in an anolyte solution containing 18 wt. % $NaBH_4$ in 17 wt. % NaOH [23].

Fig. 8 shows a comparison of the performance of a BH_4^-/O_2 fuel cell using a Au/C (2 mg Au cm^{-2}) anode catalyst combined with different cathode catalysts (2 mg material cm^{-2}). A solution containing 5 wt. % (1.32 mol dm^{-3}) $NaBH_4$ in 10 wt. % (2.5 mol dm^{-3}) NaOH was used at 85 °C in all cases. As shown in Fig. 8, the peak power density of the cell varied from 32.8 to 35.4 mW cm^{-2}, obtained when Ag/C and Ni/C were used, respectively, to 65.3 and 72.2 mW cm^{-2} obtained using iron tetramethoxyphenyl prophyrin (FeTMPP) and Pt/C, respectively [33,68].

3. Membrane materials

The ion-exchange membrane ideally prevents contact between the borohydride ions and the electrocatalytic cathode, which can be active for borohydride decomposition. The presence of borohydride ions can result in deactivation of the cathode catalyst, probably due to the formation of a borate layer on the surface. Deactivation can be minimised by using a highly selective membrane combined with the use of a cathode catalyst that is inactive towards borohydride decomposition (e.g. MnO_2), as well as an optimised concentration of fuel [14]; high concentrations of borohydride can lead to a high degree of borohydride crossover [69].

In the DBFC, an ideal anion-exchange membrane will transport hydroxyl ions from the catholyte to the anolyte compartment maintaining the alkaline pH of the anolyte at sufficiently high levels to ensure the stability of the borohydride ions, as can be seen in Fig. 9(a) and (c). If a cation-exchange membrane is used, sodium ions migrate from the anode to the cathode compartment during operation to maintain charge balance, as shown in Fig. 9(b) and (d).

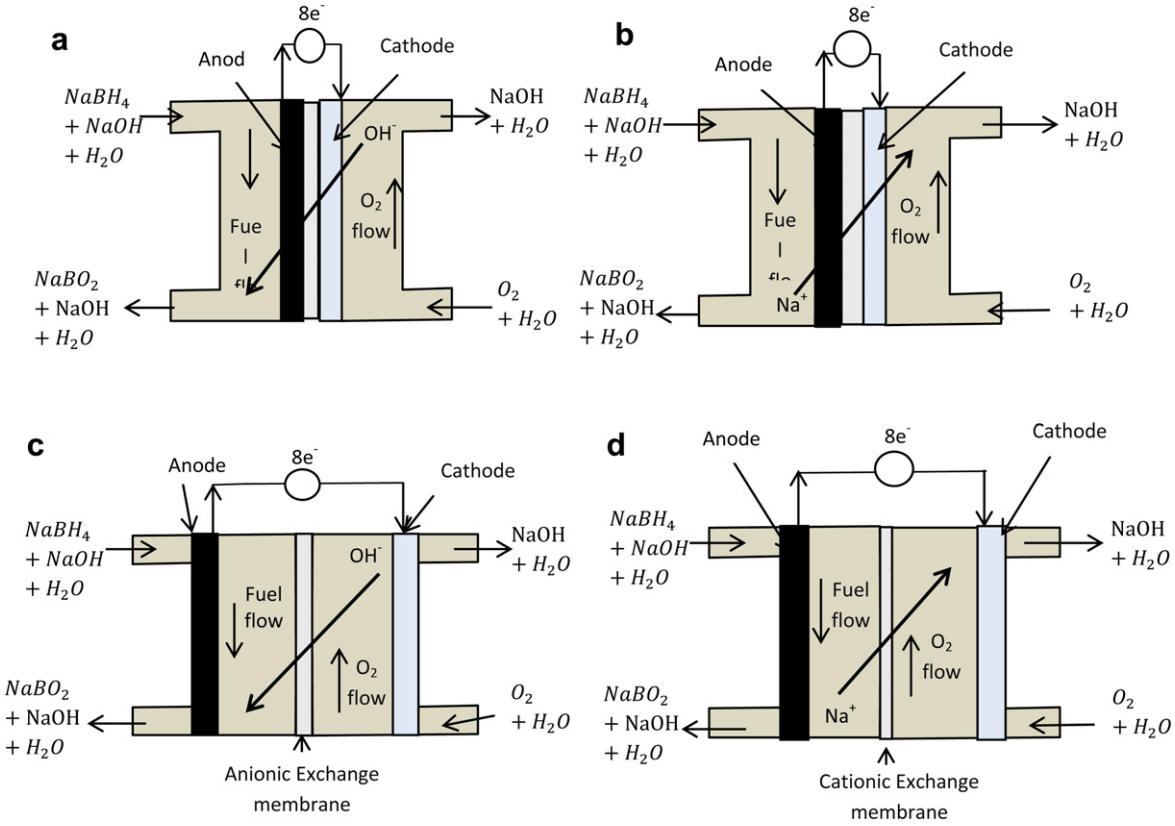

Fig. 9. Different configurations of the direct borohydride fuel cell (DBFC): MEA configuration where the electrodes are separated by: a) An anionic exchange membrane and b) A cationic exchange membrane. Oxygen reduction in an alkaline media in a flow system where the electrodes are separated by the electrolytes and by c) An anionic exchange membrane and d) A cationic exchange membrane.

The drawback of using a cation-exchange membrane (Na^+ exchange) is that the alkalinity of the anolyte decreases during operation; thus, the borohydride becomes unstable. The majority of DBFCs use cation-exchange membranes (particularly Nafion) because they severely restrict $NaBH_4$ crossover. Nafion membranes are also selected by virtue of their mechanical and chemical stabilities in strongly alkaline environments, although their long term stability is questionable, particularly at high temperatures [70]. Improved performance is obtained with thin membranes, which is due to the correspondingly lower ohmic resistance. Thin membranes, however, exhibit higher rates of borohydride ion crossover, leading to larger deviations in the open-circuit potential (OCP) from the theoretical value [16,71].

According to Raman and co-workers [57] the use of a Nafion (R)-961 membrane helps to prevent the crossover of BH_4^- [71]. Using a non-commercial membrane made from polyethylenetetrafluoroethylene (ETFE-g-PSSA), the power density and the peak current was higher than that of a DBFC using a Nafion 117 membrane. The open circuit potential, nevertheless, was found to be higher when a Nafion membrane was used [72]. Ma et al. [73] recently reported the use of a 200 μm polyvinyl alcohol hydrogel membrane (PAHM) in a DBFC with a Ni–Pt/C anode and a gold sputtered cathode using oxygen, humid air and hydrogen peroxide as oxidants. They compared their results with the equivalent experiment using a Nafion 212 membrane, and obtained lower power densities with the PAHM membranes: 218 mW cm^{-2} for Nafion 212 and 176 mW cm^{-2} for the PAHM membrane, respectively (at 60 °C), probably due to a higher crossover rate. The results, however, were slightly better with the PAHM membrane when using oxygen: 242 mW cm^{-2} at 60 °C. The stability test found that the BH_4^-/H_2O_2 fuel cell could discharge a current density of 50 mA cm^{-2} for 100 h at ambient temperature.

Ion exchange membranes tend to be expensive and complicate the cell design. They also involve a slow rate of undesirable crossover, which requires frequent replacement of the solutions. Experiments with an undivided DBFC have been reported by Feng et al. [16], who demonstrated that MnO_2 could be used as a cathode material in a membrane-less DBFC or in a DBFC using a conventional alkaline membrane rather than an expensive electrolyte membrane (e.g. Nafion). This is due to the absence of chemical reactions or crystalline transformation at the MnO_2 surface in contact with BH_4^-. A cell potential of 0.6 V and current densities between 1 and 5 mA cm^{-2} were obtained using a dispersed gold catalyzed anode (7.4–8 electrons interchanged) and a solution containing 1 mol dm^{-3} KBH_4 in 6 mol dm^{-3} KOH and a MnO_2 catalyzed air cathode. Superior performance was achieved by Verma et al. [71] who, in contrast to Feng et al. [16], used a Pt/Ni anode in a flowing alkaline electrolyte and obtained a power density of 19 mW cm^{-2} at a current density of 39 mA cm^{-2} using 1 mol dm^{-3} $NaBH_4$ in 3 mol dm^{-3} KOH.

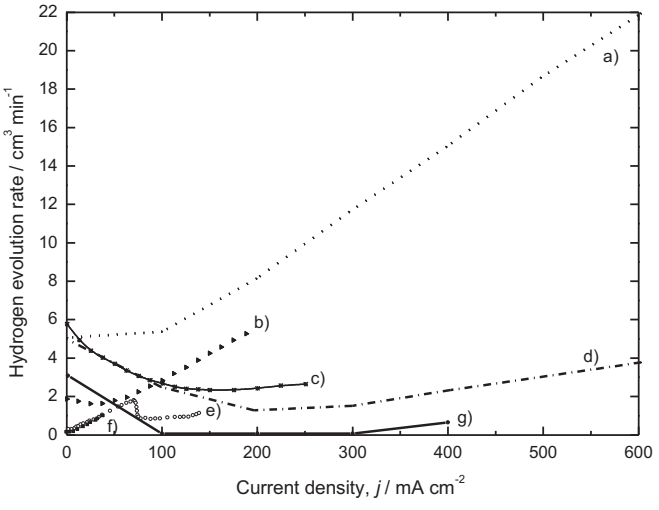

Fig. 10. Hydrogen evolution rate *vs.* anodic current. a) 1 g Ni (Inco type 210, particle size 0.5–1.0 μm), d) 10 wt. % Pd/C, g) 5 wt. % Pt/C: 0.5 mol dm^{-3} $NaBH_4$ in 6 mol dm^{-3} NaOH at room temperature [18]; b) Ni (Inco type 255, particle size 2.2–2.8 μm), c) 20 wt. % Pt/C e) 20 wt. % Au/C, f) Cu: 0.5 mol dm^{-3} $NaBH_4$ in 2 mol dm^{-3} NaOH [74].

4. Hydrogen evolution

Hydrogen evolution is a major obstacle to commercial DBFC development. A great deal of effort has been directed towards curtailing the main route to hydrogen evolution, namely, borohydride hydrolysis. Liu et al. [18] measured the volumetric hydrogen evolution rate at various anodic currents and sodium borohydride concentrations using Ni, Pd/C and Pt/C as anode catalysts. Wang et al. [74] measured the hydrogen evolution rate and the anodic current at different electrode potentials and sodium borohydride concentrations using Ni, Pt/C, Au/C and Cu. A comparison of their results, obtained for 0.5 mol dm^{-3} $NaBH_4$ in 6 mol dm^{-3} NaOH and in 2 mol dm^{-3} NaOH, respectively, is shown in Fig. 10. In all cases, the rate initially decreased at low currents but increased dramatically when high currents were applied, with the most dramatic increases observed when Ni was used. The lowest rates of hydrogen evolution at high current densities were observed on Pd and Pt electrodes, curves d) and g) respectively, however, at the open circuit potentials difference the hydrogen evolution on these metals is also significant. When the Pt/C electrode was used, Wang et al. [74] obtained a hydrogen evolution rate that was orders-of-magnitude faster than that observed by Liu et al. [18] for the same borohydride concentration (0.5 mol dm^{-3}) and approximately the same temperature. This could have been due to differences in the catalyst loading and concentration of sodium hydroxide.

It was also demonstrated in both studies that higher initial concentrations of borohydride lead to faster rates of hydrogen evolution. Liu et al. found that a quasi-$8e^-$ reaction was possible on Pt anode when the borohydride concentration was kept below 1 mol dm^{-3} in the alkaline solution [18]. The authors suggested that the number of hydride ions H^- in the tetrahedral BH_4^- ions available for adsorption on the Pt increases as the borohydride concentration is decreased, leading to a more efficient borohydride oxidation reaction. A maximum of three H^- can be absorbed simultaneously, suggesting a limit of $6e^-$ oxidation. It was conjectured that the additional $2e^-$ in the quasi-$8e^-$ regime were a result of H_2 electrooxidation. In a subsequent study, Li et al. [75] investigated whether a thin Nafion film coating on the catalyst surface could decrease the hydrogen evolution rate by lowering the surface concentration of BH_4^- ions. If the Nafion loading is too high, on the other hand, ingress of the fuel to the active sites is hindered; the optimal content was found, therefore, to be less than 25 wt. %. The hydrogen generation rate was also reduced by decreasing the temperature, which carried a penalty in terms of the cell performance [75].

Thiuorea (TU) and tetraethyl ammonium hydroxide (TEAH) have been proposed as inhibitors for the borohydride hydrolysis reaction [12]. There is a diversity of opinions on the use of TU as an inhibitor for the hydrolysis of borohydride in a DBFC. Demirci [76] suggested that the molecules of TU can block the active sites when adsorbed on the electrode surface. This limits the formation of M–H bonds and, therefore, the rate of hydrogen generation, but those sites can also be blocked for the borohydride oxidation. Jamard et al. [77] concur with Demirci, arguing that although TU reduces the hydrogen evolution rate, it also decreases the cell power at the

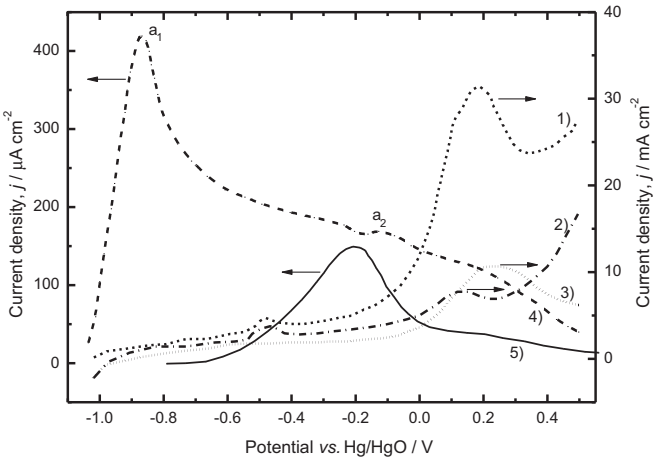

Fig. 11. Cyclic voltammogram: 1), 2), 3): 0.03 mol dm^{-3} BH_4^- + 2 mol dm^{-3} NaOH + 1.5 × 10^{-3} TU, 2 mol dm^{-3} NaOH with 1.5 × 10^{-3} TU + 2 mol dm^{-3} NaOH on colloidal 10 wt.% Os at 100 mV s^{-1} and 298 K [26]. 4), 5): Pt disc electrode (1 mm diameter) in 0.03 mol dm^{-3} $NaBH_4$ + 2 mol dm^{-3} NaOH in the absence and presence of 1.5 × 10^{-3} mol dm^{-3} of TU [20].

concentrations used. Cyclic voltammograms conducted using a three-electrode cell with a Pt disk electrode and a solution containing 0.1 mol dm^{-3} $NaBH_4$ in 1 mol dm^{-3} NaOH in the absence and in the presence of 10^{-3} and 10^{-4} mol dm^{-3} TU demonstrated that the current peak tends to decrease with an increasing concentration of TU. Polarization curves showed that when TU was added the OCP was lower than the theoretical value, and that the power peak was reduced by 50% (90 mW cm^{-2} in the presence of 10^{-4} mol dm^{-3} TU) [77].

Although all authors agree that TU inhibits the ionization and liberation of hydrogen, and does not affect the BH_4^- electrooxidation, some authors assert that the performance of the fuel cell can be improved when adding TU [78]. Fig. 11 shows cyclic voltammograms from Martins et al. [12] in the presence and in the absence of TU using a three-electrode cell consisting of Pt on a Ni mesh as the working electrode, Ag/AgCl as a reference electrode and a Pt mesh as the counter electrode. A solution of 0.03 mol dm^{-3} $NaBH_4$ in 2 mol dm^{-3} NaOH in the absence and in the presence of different concentrations of TU was used. In the absence of TU, three oxidation peaks were observed: the peak a_1 is due to oxidation of the hydrogen generated through the hydrolysis of borohydride (reactions (13) and (14)); the peak a_2 is due to the direct oxidation of BH_4^- (reaction (2)); and the third peak in the reverse cycle, c_1 (not shown for clarity), is due to the intermediate product of oxidation, BH_3OH^- (reaction (12)). In the presence of TU it was observed that the peaks a_1 and c_1 disappear, which means that TU inhibits the oxidation of H_2 and possibly the catalytic hydrolysis of BH_4^- in conjunction with the oxidation of the intermediate species (reactions (11) and (12) do not take place in this case). Only an oxidation peak at the same potential as the oxidation of BH_4^- on Pt (−0.2 V *vs.* Ag/AgCl) appears.

The effects of different concentrations of TU on the oxidation of borohydride were studied by Martins et al. [12] by adding TU at 5 × 10^{-3}, 1.5 × 10^{-2}, 2 × 10^{-2} and 3 × 10^{-2} mol dm^{-3} to a solution containing 2.6 × 10^{-2} mol dm^{-3} $NaBH_4$ in 3 mol dm^{-3} NaOH using a Pt rod as the working electrode. Cyclic voltammograms showed that when 3 × 10^{-2} mol dm^{-3} of TU was used, the oxidation peak was higher than that obtained without BH_4^-, which means that the TU could be oxidised at the same potential as the borohydride ions. Higher current values were obtained when the concentration of TU was higher (2 × 10^{-2} mol dm^{-3} compared with 1.5 × 10^{-2} mol dm^{-3}). In conclusion, the concentration of TU can improve the performance of the cell, decreasing the hydrogen evolution rate and increasing the charge efficiency; there is an optimum concentration above which the TU impacts negatively on the cell performance, decreasing the transfer current density associated with borohydride oxidation.

Celik et al. [78] showed that on addition of 1.6 × 10^{-3} mol dm^{-3} TU to 1 mol dm^{-3} $NaBH_4$ in 20 wt. % (5 mol dm^{-3}) NaOH solution and using a Pd/C electrode, the power density increased from 14.4 to 15.1 mW cm^{-2} due to the decreased rate of hydrogen evolution. Atwan et al. [26] performed cyclic voltammetry studies on supported colloidal Os using a three-electrode cell, with a graphite rod as the counter electrode and Ag/AgCl, KCl_{std} as the reference electrodes. The results are depicted in Fig. 11, together with cyclic voltammograms from electrolytes containing 2 mol dm^{-3} NaOH, 2 mol dm^{-3} NaOH with 1.5 × 10^{-3} mol dm^{-3} TU, and 0.03 mol dm^{-3} $NaBH_4$ in 2 mol dm^{-3} NaOH with 1.5 × 10^{-3} mol dm^{-3} TU on 10 wt. % Os. The oxidation potentials of TU and BH_4^- appear to be between 0.1 and 0.3 V *vs.* Ag/AgCl, KCl_{std}, meaning that they both oxidise at the same potential and the oxidation wave is a mixture of both the TU and BH_4^- oxidation currents.

TEAH, in contrast to TU, does not eliminate the voltammetric responses due to hydrogen evolution. Instead, it shifts the oxidation peak of the borohydride ions by +0.3 V, which could be due to adsorption of the TEAH ion on the Pt electrode, decreasing the hydrogen oxidation reaction rate in alkaline media [20]. Clearly, there is scope for an *in-situ* surface electrosorption study using, e.g., FTIR/Raman spectroscopy.

5. Performance and the effect of operational variables

5.1. Effects of temperature on DBFC performance

One advantage of borohydride fuel cells is their capability to provide energy at (or near) room temperature, which makes them suitable for portable applications. There is evidence, on the other hand, that performance improves at elevated temperatures [43,79]. The power density and the sustained current density increase with increasing temperature. Increasing the temperature presents some advantages, such as improved mass transport of the reactants, faster kinetics of borohydride electrooxidation and increased ionic conductivities of the electrolytes/membrane. High temperatures, however, enhance the crossover rate and the hydrolysis of BH_4^-, which means a lower fuel utilization and deterioration in the activity of the cathode. These effects are manifested in a lower OCP. A secondary problem with elevated temperatures is dehydration of the membrane, which increases the membrane resistance and severely diminishes performance [44,69]. Ma et al. [44] conducted experiments in a borohydride fuel cell comprising a Nafion® 212 membrane, a Ni + Pd/C compositae anode, and 1 mg cm^{-2} Pt/C in the cathode. The fuel was 5 wt. % (1.32 mol dm^{-3}) $NaBH_4$ and 10 wt. % (2.5 mol dm^{-3}) NaOH aqueous solution, with a flow rate of 5 dm^3 min^{-1}. The oxidant was humidified oxygen or humidified air with a flow rate of 0.15 dm^3 min^{-1}. The power density increased from 77 mW cm^{-2} to 167 mW cm^{-2} by increasing the temperature from 28 °C to 60 °C. The increase in temperature, however, will also cause an increase in the hydrogen evolution rate, which was not quantified [80].

5.2. Effects of reactant concentrations on DBFC performance

According to the Nernst equation, the OCP would be expected to increase with an increased concentration of BH_4^-. Experiments have shown that an increase in the $NaBH_4$ concentration improves the performance of the anode but also increases the cathode polarization [32], probably as a result of increased borohydride crossover.

The rate at which the cathode polarization increases is diminished as the concentration of borohydride ions is increased [18]. Cheng and Scott [69] performed experiments in a $NaBH_4/O_2$ fuel cell with a Nafion® 117 membrane, 2 mg cm^{-2} Au/C anode, 2 mg cm^{-2} Pt/C cathode with solutions containing concentrations of $NaBH_4$ of 3, 5, 8 and 10 wt. % (0.79, 1.32, 2.1 and 2.64 mol dm^{-3}) in 10 wt. % (2.5 mol dm^{-3}) NaOH. The peak power density increased by around 30% when the concentration of borohydride increased from 3 wt. % to 5 wt. %, but did not increase appreciably with further increases in the concentration; an increase of 10% was achieved by further doubling the borohydride concentration to 10 wt. %. This is not surprising, considering that the Au loading was kept constant. The power density and current density rose by 10% when the NaOH concentration was increased from 5 to 10 wt. % (1.25 mol dm^{-3} to 2.5 mol dm^{-3}) but it decreased when the NaOH concentration was further increased to 20 wt. % (5 mol dm^{-3}).

To summarize, increasing the concentration of borohydride: (a) alleviates mass transport limitations, which leads to higher power densities and higher current densities; (b) increases the borohydride crossover rate [69,81] and leads to hydrogen evolution [82], which negatively impacts on the cathode performance, causes fuel loss and reduces the OCP [69]. Moreover, the current density is limited by the catalyst loading, so that continually increasing the fuel concentration will yield diminishing returns. Hence, the concentration of fuel should be optimised, taking into account the cell performance and the cost of the fuel. Likewise, the concentration of NaOH should be considered because it will influence the conductivity and alkalinity of the solution (ohmic losses, particularly through the electrolytes and membrane, are high). A high sodium hydroxide concentration increases the viscosity of the solution and reduces the mobility of Na^+ ions [6], also hindering the movement of borohydride ions towards the reaction sites [32]. By increasing the concentration of NaOH, the fuel crossover rate decreases as a result of the increased numbers of migrating Na^+/OH^- ions blocking the passage of borohydride ions through the membrane [69].

5.3. Effects of fuel flow rate on DBFC performance

The fuel/oxidant flow rate is another factor that affects the DBFC performance. Experiments with oxidant (humidified air; 65% RH, 1 atm) flow rates of 10, 20, 90 and 150 cm^3 min^{-1} were carried out by Celik et al. [47] using a 25 cm^2 cell consisting of a Pd/C anode, a Pt/C cathode and a Nafion membrane. Analysing the polarization curves it was found that increasing the flow rate of the oxidant led to small increases in the power density (8.5 and 10.1 mW cm^{-2} at 10 and 150 cm^3 min^{-1}, respectively). Kim et al. [83], on the other hand, increased the power density of the cell by 21% by increasing the oxidant (air) flow rate from 5 to 10 dm^3 min^{-1} and keeping a constant fuel flow rate of 0.108 dm^3 min^{-1}. Clearly, low flow rates (<10 dm^3 min^{-1}) will engender high polarizations as a result of oxidant depletion, and are not, therefore, practical.

Cheng and Scott [69] carried out experiments at different fuel flow rates (10–200 cm^3 min^{-1}) using carbon supported Au and Pt catalysts assembled in a 4 cm^2 active area MEA. They concluded that a higher flow rate improves the performance of the cell by promoting better mass transport of the fuel and reducing possible channel blocking and product accumulation [69]. Duteanu et al. [11] argued that the effect of the anolyte flow rate on the fuel cell performance is small and it is more economical to use low flow rates.

Higher fuel rates will undoubtedly improve the mass transfer characteristics and lead to more uniform reactant distributions in the cell (important for avoiding dead zones of low reactant concentration and, ultimately, regions of high overpotential). A higher flow rate may also improve mass transport by removing the evolved hydrogen gas more effectively. There will be an optimal flow rate, however, above which improvements in performance are not compensated by the additional pumping power required. Higher flow rates also place additional stresses on the electrode materials, sealing materials and piping, increasing the risk of electrolyte leakage.

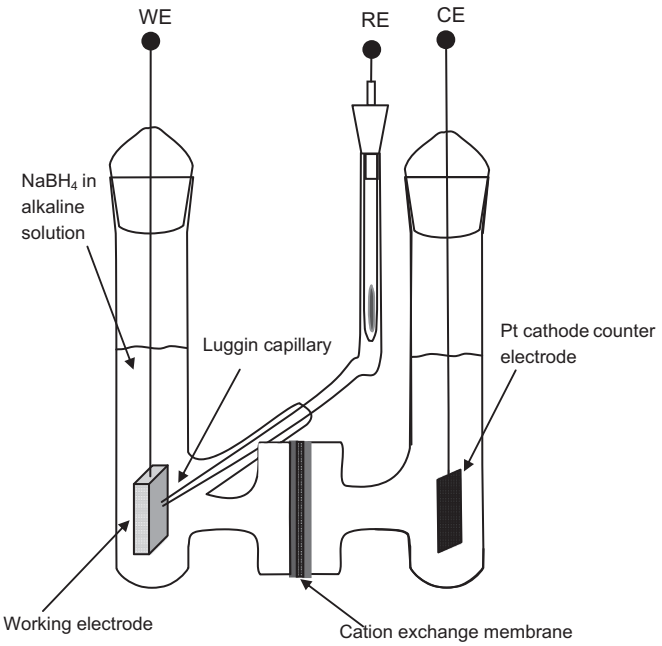

Fig. 12. Typical three-electrode glass cell to carry out fundamental voltammetric studies of the borohydride oxidation reaction such as kinetic rate constants, exchange current densities and mass transport characteristics [64].

6. Engineering aspects of direct borohydride fuel cells

Different flow cell designs have been investigated for the DBFC in order to improve its performance. Half-cell designs such as the typical three-electrode cell, shown in Fig. 12, are typically used to calculate the kinetic parameters. This electrochemical cell comprises working, counter and reference electrodes, with the counter electrode in a different compartment separated by a membrane [64].

The anode and cathode can be placed facing each other as in Fig. 9(c) and (d). The ion-exchange membrane can also be sandwiched between the anode and cathode forming a membrane electrode assembly (MEA), as shown in Fig. 9(a) and (b). In both cases the fuel, sodium borohydride in alkaline solution, and the oxidant, either hydrogen peroxide solution, air, or pure oxygen, are pumped from separate tanks to the anode and cathode compartments, respectively. The fuel and oxidant pass through the flow field plates, normally made of graphite or stainless steel, towards the anode and cathode and react to exchange a maximum of 8 electrons [8]. The hydrogen gas, primarily from borohydride hydrolysis, will pass through the flow fields together with the borohydride solution, decreasing the ionic conductivity of the electrolyte and the effective diffusion coefficients of the reactants.

Serpentine and parallel flow channels are the most commonly used flow field designs for direct liquid fuel cells. A serpentine channel is typically used in the anode, since it promotes better mass

transport of the fuel. Long narrow channels will increase the gas–liquid flow difficulties, the pressure losses and any fluctuations, which can cause failure of the cell due to unstable system operation. A serpentine flow field can also reduce the degree of channel blocking [84]. Cheng and Scott [69] increased the power density of a DBFC by 3.5% when moving from a parallel to a serpentine flow field.

Kim et al. [83] used a parallel flow field in the anode compartment and a serpentine flow field in the cathode; the anode catalyst was a Zr-based AB_2-type H_2 storage alloy and the cathode catalyst was 5 wt. % Pt/C. A Nafion 115 membrane was used to separate the electrodes. They obtained a current density of 420 mA cm^{-2} and a power density of 218 mW cm^{-2}. The experiment was carried out in a system containing a solution of 10 wt. % (2.64 mol dm^{-3}) $NaBH_4$ in 20 wt. % (5 mol dm^{-3}) NaOH fed to the anode at 0.025 dm^3 min^{-1} and humidified air fed to the cathode at 10 dm^3 min^{-1}. They increased the power of the fuel cell by 56% when a gold anticorrosion coating on the stainless steel end plates and on the Ni mesh was used, which protected the plates during operation. In a normal MEA, a dead zone can be formed in the anode as a consequence of the generation of hydrogen, which blocks the access of the fuel to the anode [83]. This problem can be alleviated by evacuating the hydrogen bubbles by, for example, leaving a gap between the anode and the membrane through which the hydrogen bubbles can easily escape from the anode. Kim et al. [83] increased the power density of the cell by 27% by using a corrugated-shaped anode separated from the membrane by 2 mm, applying an anticorrosion coating on the cathode channel, and controlling the fuel flow-rate and air humidity. It is thought that humidification of the air helps to remove the accumulation of sodium hydroxide on the surface of the cathode catalyst. Park et al. [85] reported that DBFC performance improves at higher flow rates by virtue of a more efficient removal of hydrogen bubbles from the channels of the anode fuel flow field. The hydrogen bubbles decrease the ionic conductivity of the electrolyte and the effective diffusion coefficients of the reactants, negatively impacting on cell performance, mainly at low flow rates.

6.1. Stack configuration

The fuel cell stack consists of:

a) Single cells, where the fluid flow field plates are placed on each side of a MEA to form the anode and cathode compartments. The plates provide channels through which the reactants and products flow, and also function as current collectors. In the stack, the adjacent anode and cathode flow field plates usually function as bipolar plates. If two or more single cells are placed side by side, a mono-polar strip stack is formed, where air can be fed to one side of the stack by spontaneous convection [86].
b) Bipolar electrode cells, formed by two cells by interfacing the anode of one and cathode of the other, separated by a space, where fuel and products flow. The union of two or more of bipolar-cells is known as a bipolar cell stack [86].

The different configurations of fuel cell stacks are shown in Fig. 13(a) and (b), in which the fuel is fed in parallel and in series, respectively. Since the performance of DBFCs improves with increasing temperature, electrical heaters are often placed behind the graphite blocks to heat the cells to the desired temperature.

In order to obtain higher output powers, a large number of cells can be stacked together. By increasing the number of cells, however, the weight and volume also increase, and this has to be taken into account during cell design. Kim et al. [87] assembled a five-cell stack using corrugated anodes with 5 wt. % Pt on a carbon cloth substrate, cation-exchange membranes and a gold-coated stainless steel mesh to form MEAs of 72 cm^2 effective area. A parallel flow field was used for the anode and a serpentine flow field for the cathode. A solution of 10 wt. % (2.64 mol dm^{-3}) $NaBH_4$ in 20 wt. % (5 mol dm^{-3}) NaOH was fed the anode and air was fed to the cathode. The authors obtained 200 mW cm^{-2} using the stainless steel end plates, which was reduced by 12% when carbon graphite end plates were used. The endplates were tightened using mechanical pressure to ensure full contact between the bipolar plates; the applied force was higher on the stainless steel plates than on the carbon graphite plates and the weight decreased by

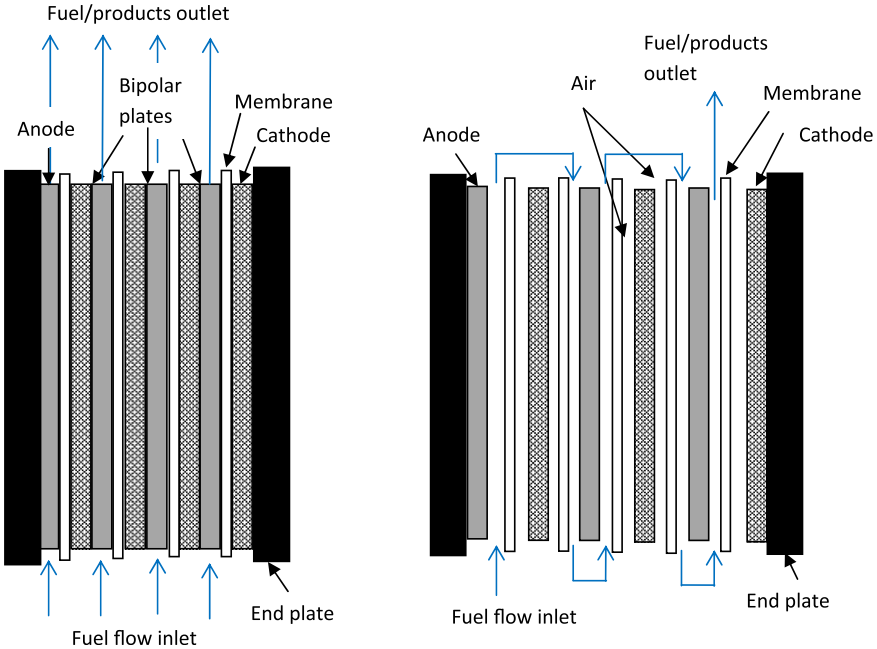

Fig. 13. Different configurations of flow arrangements in a bipolar flow cell: a) 4-Cell stack with the reactant flow circuit feed in series and b) A 5- cell stack with the reactant feed in parallel flow circuit.

a factor of 4.2 when the graphite endplates were used. The thickness of the plates is an important factor here because the stainless steel plates can be much thinner, leading (usually) to a lower weight and a smaller volume. However, stainless steel can experience slow corrosion resulting in the leaching of transition metal ions, including Fe, Cr and Ni, which can accelerate the contamination and degradation of PFSA membranes, particularly in the cathodic acid side of the cell. In the alkaline anode environment, the stainless steel experiences low corrosion rates due to passivation. High-grade stainless steel can be used to decrease the corrosion rate in the cathode side but incurs additional costs.

7. Modelling and simulation

An ideal model of the direct borohydride–oxygen fuel cell would incorporate:

a) The highly complex borohydride oxidation reaction.
b) The competitive hydrolysis reaction.
c) The cathode electrochemical reaction(s).
d) Reactant transport (via diffusion, migration and convection).
e) Charge transport in the solution, membrane and electron-conducting media.
f) The influence of gas bubbles on reactant and charge transport in the solutions.
g) Reactant crossover and mixed potentials arising from competing reactions in the electrodes.
h) Heat generation and transport through the cell.
i) The influence of geometry on performance.
j) Steady state and dynamic performance.

Modelling could play a critical role in improving fundamental understanding, offering key information on, or confirming the roles played by the electrochemical reactions, the transfer/transport of reactants, charge and heat, and the distributions of the current, potential and concentrations of electroactive species and intermediates. In identifying promising designs, modelling can be used in conjunction with experimental studies to accelerate progress, reducing the costs and timescales associated with laboratory tests. Thus far, however, very few models of borohydride fuel cells have been developed.

Verma and Basu [88] developed a highly simplified mathematical steady-state model to predict the fuel cell potential at a given current density in a O_2 DBFC. The model assumed an anode reaction mechanism proposed by Morris et al. [22] in their half-cell studies on Pt electrodes:

$$BH_4^- \leftrightarrow HBO_{2ad} + 5H_2O + 8e^- \quad (26)$$

$$OH^- \leftrightarrow OH_{ad} + e^- \quad (27)$$

$$HBO_{2ad} + OH_{ad} + e^- \rightarrow BO_2^- + H_2O \quad (28)$$

The concentrations of BH_4^- and OH^- and the fractional coverages of the adsorbed intermediates were calculated via simple steady-state balances with fixed rate constants, and the first two were used to estimate the activation overpotential in the anode by inverting a Tafel relationship. The cathode overpotential took into account oxygen diffusion across the gas diffusion layer (linearization of Fick's law), to estimate the surface concentration. This however, ignores the diffusion layer in the catalyst layer, which is the overwhelming source of mass transfer limitations. Ohmic resistances were modelled by estimating an 'overall' resistance from experimental data, at different temperatures. To obtain a reasonable qualitative fit to the data, an additional ad-hoc term representing the concentration polarization in the anode was required. The discrepancies could have been eliminated with proper consideration to the mass transfer resistances at both electrodes, particularly through the catalyst layers.

Sanli et al. [89] developed a series of similarly simplified model for the BH_4^-/H_2O_2 DBFC, again ignoring mass, charge and heat transport. The three models differed only in the manner in which the concentration overpotentials were incorporated and whether the cathode was include in the model. Relationships for the activation overpotential were again based on Tafel laws applied to each electrode and concentration overpotentials were derived by including reactant concentrations in the Tafel expression or by introducing a limiting current density. The ohmic losses were characterised by a constant resistance, estimated experimentally along with the reaction constants and the OCP. The range of current density considered was narrow, up to 0.02 A cm^{-2} (similar to that considered by Verma et al.), and only by including the cathode explicitly was a reasonable fit to the data possible. Models of this level of simplicity can perhaps provide a means of monitoring performance but lack the physical detail required for design purposes. In particular, material properties, solution compositions, geometry and operating conditions are crucial to the performance of DBFC (as detailed in previous sections).

Quantum mechanical models can be used to elucidate the reaction mechanism on heterogeneous catalysts by quantifying the structure and energy density of stable states and transition states along a reaction coordinate (representing the transformation of reactant to products). Density functional theory (DFT) is widely used to analyse the reactivity of metal and metal-oxide surfaces. Rostamikia and Janik [36] applied a range of DFT approaches to evaluate aspects of the reaction mechanism of borohydride oxidation on Au (111) and Pt (111) crystalline surfaces [90,91]. The authors found that the molecular adsorption of borohydride ions on Au(111) is only favourable at high overpotentials, whereas initial adsorption over the Pt(111) surface is dissociative and highly favourable at all potentials of interest. They also concluded that hydrogen evolution is favourable on Pt(111) surface, and Pt electrodes have promote B–H bond cleavage and B–O bond formation reactions. The activation barriers for O–H dissociation, on the other hand, were high, leading to boric acid as the preferred final surface oxidation product [91]. Overall, the activity of Au electrodes was limited by a low coverage of reaction intermediates due to the weak adsorption mentioned above, whereas oxidation on Pt electrodes was limited by strong dissociative adsorption, which promoted hydrogen evolution. It must be noted that the electrode was represented by a single crystal surface and that the desorption of intermediate species from the surface (and any subsequent solution-based reactions) were not considered in the model. Rostamikia et al. used the same methods to approximate potential-dependent rate constants for a mechanism on Au(111) using a Butler-Volmer formalism and transition-state theory [92]. These rate constants were then used in a kinetic model (for the surface coverage of species) based on an overall oxidation reaction that proceeds through the minimum energy path determined through the DFT studies [90,91]. Linear sweep voltammograms were simulated and the results suggested that B–H containing species are stable surface intermediates at electrode potential where an oxidation current is observed. The presence of BH_3 as a stable intermediate was confirmed by surface-enhanced Raman spectroscopy [92].

8. Recycling sodium metaborate product to sodium borohydride reactant

The oxidation of borohydride is an irreversible reaction yielding a complex mixture of borates and metaborates as products.

Different chemical routes exist to recycle these products, which could potentially make the borohydride fuel cell a sustainable process. Kojima and Haga [15] investigated the reaction of $NaBO_2$ with MgH_2 obtaining yields between 4.8 and 97% for pressures between 0.5 and 7 MPa, at a temperature of 550 °C. The authors found that the yield of $NaBH_4$ obtained from reaction (29) increased with temperature and pressure but was independent of the reaction time (obtaining the same yield in 2- and 4-h experiments). According to Wu et al. [93] this method has not been developed far enough to offer both high yield and fast reaction rates. The proposed reaction is:

$$NaBO_2 + 2MgH_2 \rightarrow NaBH_4 + 2MgO \quad (29)$$

$NaBH_4$ can also be generated from $NaBO_2$ using MgSi under high H_2 pressure. The yield obtained was 98% at 550 °C under 7 MPa and increased with temperature, although it was the same after 4 h of operation [15]:

$$NaBO_2 + 2Mg + Si + 2H_2 \rightarrow NaBH_4 + 2MgSi + 2H_2 \quad (30)$$

$$NaBO_2 + Mg_2Si + 2H_2 \rightarrow NaBH_4 + 2MgO + Si \quad (31)$$

Coke, as shown in reaction (32), or methane (reaction (33)), can also be used to generate $NaBH_4$ from $NaBO_2$ [15]:

$$NaBO_2 + 2C + 2H_2O \rightarrow NaBH_4 + 2CO_2 \quad (32)$$

$$NaBO_2 + 2CH_4 + 2H_2O \rightarrow NaBH_4 + 2CO_2 + 4H_2 \quad (33)$$

Methane is an inexpensive reducing agent and would generate $NaBH_4$ from $NaBO_2$ in a one step process (reaction (33)). The free energy of this reaction, however, is large and positive at temperatures between 0 and 1000 °C, which precludes its use for the synthesis of sodium borohydride. For the same reasons, coke or H_2 are not used as reducing agents to generate $NaBH_4$ from $NaBO_2$ [93].

Sanli et al. [94] studied the use of hydrogen as a reducing agent to generate sodium borohydride. The authors presented a cyclic voltammogram of a solution containing 0.1 mol dm^{-3} $NaBO_2$ in 1 mol dm^{-3} NaOH on an Ag gauze electrode, finding a reduction peak at 0.5 V *vs.* SCE. Constant potential electrolysis at 0.5 V *vs.* SCE during 24 and 48 h at room temperature was employed in order to synthesise borohydride via the following reaction mechanism:

$$BO_2^- + 4H_2 \rightarrow BH_4^- + 2H_2O \quad (34)$$

$$2H_2O + 2e^- \leftrightarrow 2OH^- + H_2 \quad (35)$$

$$2OH^- + 2H^+ \leftrightarrow 2H_2O \quad (36)$$

After the electrolysis, a new peak at −0.2 V *vs.* SCE was found in the cyclic voltammogram. The height of the peak increased with the time of electrolysis and after comparing the CV with that of the same solution with an added 10 dm^3 of $NaBH_4$, it was confirmed that the peak was due to the generation of $NaBH_4$ from $NaBO_2$. The reaction was followed by iodometric titration, resulting in 9% conversion of $NaBO_2$ into $NaBH_4$ after 24 h of electrolysis and 17% conversion after 48 h. Similar experiments were conducted with an Au catalyst, exhibiting similar results, except that the new peak due to borohydride oxidation was shifted to −0.1 V *vs.* SCE [94]. Gyenge and Oloman [95] carried out experiments on the electroreduction of borates under both electrocatalytic hydrogenation and direct electroreduction conditions in alkaline media, showing no measurable amounts of BH_4^-. The authors also questioned the use of the iodate method to analyse the concentration of borohydride ions because the medium was not acidic enough.

The electroreduction of borates in aqueous media has also been reported in the literature [96–99]. The electrolytic production of sodium borohydride in water, however, is not likely to be feasible due to the very slow reaction kinetics. A lower energy is required to reduce the water to hydrogen than is required to reduce the metabororates at the cathode and the oxygen at the anode. If high overpotential materials are used at the cathode, the hydrogen evolution reaction will be avoided but these materials do not exhibit activity towards sodium borohydride generation [93].

9. Summary

The DBFC is a promising power source but many constructional and operational aspects of the cell still need to be improved for it to become a reliable energy source. These include:

a) Finding an appropriate, preferably low-cost, anode catalyst to achieve an eight (or close to eight) electron transfer, while minimizing borohydride hydrolysis.
b) Minimizing reactant crossover or engineering cathode catalysts that are not active towards borohydride oxidation, perhaps allowing the membrane to be eliminated altogether.
c) Increasing the current density.

Although it has been claimed that Au catalyzes the borohydride oxidation close to completion and avoids the unwanted hydrolysis reaction, higher peak power densities have been obtained with Pd/C anodes. For example, it has been shown that a Pd/C anode (2 mg Pd cm^{-2}) is capable of producing 89.6 mW cm^{-2}, compared to 72.2 mW cm^{-2} for Au/C (also 2 mg Au cm^{-2}), both in a BH_4^-/O_2 fuel cell operating with 1.32 mol dm^{-3} $NaBH_4$ in 2.5 mol dm^{-3} NaOH at 85 °C [33,34]. Low-cost copper electrodes in the form of a flat plate and a mesh have also been used to oxidise borohydride; a maximum current density of 235 mA cm^{-2} and a peak power density of 46 mW cm^{-2} were obtained in a cell containing 2 mol dm^{-3} $NaBH_4$ in 2 mol dm^{-3} NaOH at room temperature. The cathode was a platinum electrode in a hydrogen peroxide solution separated from the anolyte by an NRE-212 membrane and the anode consisted of a stack of three copper mesh layers (200 ppi, 74 μm strand diameter) [48]. The complete anodic oxidation of borohydride in a general reaction environment, however, remains elusive and further investigations are needed to find a suitable catalytic material.

The performance of the cell also depends on the cathode materials, especially the catalyst. It has been demonstrated that the cathode polarization losses can be higher than those of the anode [30–32]. Several materials have been investigated in order to find the most appropriate cathode catalyst. As an example, the peak power density can be increased from 49.6 mW cm^{-2} to 77.3 mW cm^{-2} by using Pt/C rather than Ag/C (2 mg metal cm^{-2}) [33]. Power densities of 680 mW cm^{-2} and 1440 mW cm^{-2} have been obtained using a BH_4^-/H_2O_2 fuel cell with an electrodeposited palladium layer at the anode and a sputtered gold catalyst layer at the cathode [2,23].

The most common membrane used is the Nafion 117 cationic membrane, which possesses excellent mechanical and chemical stability in strongly alkaline media. Other types of membrane, such as the Nafion (R)-961, have also exhibited reasonable performance. The latter membrane mitigates the crossover of BH_4^- [71]. The non-commercial membrane polyethylenetetrafluoroethylene (ETFE-g-PSSA) increases the power density and the peak current of the fuel cell but simultaneously decreases the open circuit potential difference [72,73]; this is not necessarily a problem if the peak

power density increases. Membrane-less DBFCs will be a viable option if an appropriate cathode catalyst, i.e., one that is not active towards borohydride oxidation, can be found. One such candidate is MnO_2 [16], which, however, exhibits low power densities [71].

In order to suppress hydrogen evolution via the hydrolysis of borohydride, additives such as TU or TEAH have been used in the alkaline solution. Different conclusions have been reached by various authors; most agree on the ability of TU to inhibit borohydride hydrolysis, but they do not agree on whether the addition of TU will be beneficial for overall cell performance [12,74–78]. In the presence of TEAH, the oxidation peak of the borohydride ions is shifted by 0.3 V towards more positive potentials and the hydrogen oxidation rate is decreased in alkaline media [20].

The performance of DBFCs can also be improved by varying the operating conditions as follows:

a) Increasing the temperature, which enhances both the current and power densities. The diffusion coefficients of the reactants and the electrolyte conductivities increase with increasing temperature. The borohydride ions will be oxidised at a faster rate, but the rate of hydrogen generation will also increase [44,69,80].
b) Increasing the concentration of borohydride ions, which increases the current density, but also the rates of hydrogen generation and borohydride crossover (leading to higher cathode polarizations). An increase in the concentration of hydroxide ions will reduce the rate of crossover, but will also increase the solution viscosity, decreasing the rates of reactant diffusion and increasing ohmic losses through the electrolytes, particularly at high current densities [32,69,81].
c) Increasing the fuel flow rate, which improves performance by improving reactant transport in the electrodes and reducing channel blocking due to the accumulation of products [11,47]. Kim et al. [83] have shown that the performance of the cell is also affected by the air/H_2O_2 flow rate.

The cell design and construction are also key aspects requiring attention. Plate designs with appropriate flow fields for liquid solutions should be optimised for best performance, while avoiding mass-transport issues such as channel blocking. Better results were obtained when using a serpentine flow field rather than the parallel flow field [69,84]. Kim et al. [83] improved cell performance by 27% with the use of a corrugated anode separated from the membrane by a 2 mm gap, in order to allow the gas generated to escape without blocking the anode reaction sites.

The development of models taking into account the reaction environment, mass, charge and heat transport, together with the complex reactions at the electrodes requires a detailed, physics-based approach. This area of research offers many opportunities since systematic parametric studies could point towards optimal designs (including in relation to materials and geometries) and operating conditions, avoiding expensive and time-consuming trial-and-error experimental procedures.

Although different methods for generating sodium borohydride from sodium metaborates have been developed, further investigations are required in order to obtain higher efficiencies with fast kinetics [15,93].

10. Further work

Borohydride fuel cells are potentially sustainable, clean and efficient sources of power in an energy economy that is less reliant on fossil fuels. As power sources for portable electronic equipment, they would possess significantly higher capacities than rechargeable batteries. There are, however, a number of challenges that must be overcome before DBFCs can compete with incumbent technologies. Ultimately, the aim is to increase the energy densities obtained, which are still far from the theoretically predicted values. In order to achieve this aim, further work should be concentrated on challenges such as:

1) Minimizing borohydride hydrolysis and borohydride crossover.
2) Achieving a better understanding of borohydride oxidation in order to engineer better catalysts and select optimal operating conditions, e.g., if large currents are drawn from the anode, complete anodic oxidation can be managed [6].
3) Improving the cathode performance.
4) Achieving a better understanding of the various mass and charge transport losses in DBFCs under different conditions and for different designs and materials, in order to identify areas for improvement.
5) Crystallization of borates on the anode surface and blocking of active sites.
6) The reuse and recycling of borohydride fuel and its reaction products.

Electrocatalysts that promote borohydride oxidation with the release of 8 electrons, while suppressing hydrolysis, remains very limited and there is a need for quantitative studies via, e.g., combinatorial techniques allied to molecular modelling. Further development of practical and stable, cost-effective, coated three-dimensional supports, is important. There is clearly a role for *in-situ* surface spectroscopy techniques in the elucidation of electrosorption effects on borohydride oxidation and hydrolysis in view of the poor understanding of reaction intermediates and the effects of electrolyte additives (including suppressants of hydrogen evolution and electrode promotion or poisoning).

There is a noticeable paucity of work on the characterisation of reaction environments in DBFCs, including global and localised studies of pressure drops and concentration, temperature and potential distributions within the cell components. Detailed mathematical models and simulation tools, used alongside experimental procedures such as impedance spectroscopy, would be invaluable for gaining insight into such phenomena. Currently, however, modelling and simulation have not played a significant part in DBFC development, in contrast to the extensive and detailed modelling of other electrochemical energy conversion technologies such as PEM fuel cells [100] and redox flow batteries [101].

References

[1] C. Ponce de Leon, F.C. Walsh, D. Pletcher, D.J. Browning, J.B. Lakeman, J. Power Sources 155 (2006) 172–181.
[2] G.H. Miley, N. Luo, J. Mather, R. Burton, G. Hawkins, L. Gu, E. Byrd, R. Gimlin, P.J. Shrestha, G. Benavides, J. Laystrom, D. Carroll, J. Power Sources 165 (2007) 509–516.
[3] J.P. Elder, A. Hickling, Trans. Faraday Soc. 58 (1962) 1852–1864.
[4] M.E. Indig, R.N. Snyder, J. Electroanal. Chem. 109 (1962).
[5] D.M.F. Santos, C.A.C. Sequeira, Renew. Sust. Energy Rev. 15 (2011) 3980–4001.
[6] B.H. Liu, Z.P. Li, J. Power Sources 187 (2009) 291–297.
[7] C. Ponce de León, F.C. Walsh, Encyclopedia of Electrochemical Power Sources (2009) 192–205.
[8] J. Ma, N.A. Choudhury, Y. Sahai, Renew. Sust. Energy Rev. 14 (2010) 183–199.
[9] D. Pletcher, A First Course in Electrode Processes, RSC, Cambridge, UK, 2009.
[10] B.H. Liu, S. Suda, J. Power Sources 164 (2007) 100–104.
[11] N. Duteanu, G. Vlachogiannopoulos, M. Shivhare, E. Yu, K. Scott, J. Appl. Electrochem. 37 (2007) 1085–1091.
[12] J.I. Martins, M.C. Nunes, R. Koch, L. Martins, M. Bazzaoui, Electrochim. Acta 52 (2007) 6443–6449.
[13] D.A. Finkelstein, N.D. Mota, J.L. Cohen, H.c.D. Abruna, J. Phys. Chem. C 113 (2009) 19700–19712.
[14] U.B. Demirci, J. Power Sources 172 (2007) 676–687.
[15] Y. Kojima, T. Haga, Int. J. Hydrogen Energy 28 (2003) 989–993.

[16] R.X. Feng, H. Dong, Y.D. Wang, X.P. Ai, Y.L. Cao, H.X. Yang, Electrochem. Comm. 7 (2005) 449–452.
[17] M.V. Mirkin, H. Yang, A.J. Bard, J. Electrochem. Soc. 139 (1992) 2212–2217.
[18] B.H. Liu, Z.P. Li, S. Suda, Electrochim. Acta 49 (2004) 3097–3105.
[19] E. Gyenge, M. Atwan, D. Northwood, J. Electrochem. Soc. 153 (2006) A150–A158.
[20] E. Gyenge, Electrochim. Acta 49 (2004) 965–978.
[21] S.-M. Lee, J.-H. Kim, H.-H. Lee, P.S. Lee, J.-Y. Lee, J. Electrochem. Soc. 149 (2002) A603–A606.
[22] J.H. Morris, H.J. Gysling, D. Reed, Chem. Rev. 85 (1985) 51–76.
[23] L. Gu, N. Luo, G.H. Miley, J. Power Sources 173 (2007) 77–85.
[24] S.C. Amendola, P. Onnerud, M.T. Kelly, P.J. Petillo, S.L. Sharp-Goldman, M. Binder, J. Power Sources 84 (1999) 130–133.
[25] M. Chatenet, F. Micoud, I. Roche, E. Chainet, J. Vondrák, Electrochim. Acta 51 (2006) 5452–5458.
[26] M.H. Atwan, D.O. Northwood, E.L. Gyenge, Int. J. Hydrogen Energy 30 (2005) 1323–1331.
[27] R.R. Bessette, M.G. Medeiros, C.J. Patrissi, C.M. Deschenes, C.N. LaFratta, J. Power Sources 96 (2001) 240–244.
[28] R.R. Bessette, J.M. Cichon, D.W. Dischert, E.G. Dow, J. Power Sources 80 (1999) 248–253.
[29] N. Luo, G.H. Miley, K.-J. Kim, R. Burton, X. Huang, J. Power Sources 185 (2008) 685–690.
[30] Z.P. Li, B.H. Liu, K. Arai, S. Suda, J. Electrochem. Soc. 150 (2003) A868–A872.
[31] N.A. Choudhury, R.K. Raman, S. Sampath, A.K. Shukla, J. Power Sources 143 (2005) 1–8.
[32] Z.P. Li, B.H. Liu, K. Arai, K. Asaba, S. Suda, J. Power Sources 126 (2004) 28–33.
[33] H. Cheng, K. Scott, K. Lovell, Fuel Cells 6 (2006) 367–375.
[34] H. Cheng, K. Scott, J. Appl. Electrochem. 36 (2006) 1361–1366.
[35] B. Molina Concha, M. Chatenet, Electrochim. Acta 54 (2009) 6130–6139.
[36] G. Rostamikia, M.J. Janik, Energy Enviro. Sci. 3 (2010) 1262–1274.
[37] B.M. Concha, M. Chatenet, E.A. Ticianelli, F.H. Lima, R.D. Lima, In Situ Infrared Study of the Mechanism of Borohydride Oxidation Reaction, ECS Meeting Abstracts, 902 (2009) 368.
[38] D.M.F. Santos, C.A.C. Sequeira, Electrochim. Acta 55 (2010) 6775–6781.
[39] M. Chatenet, F.H.B. Lima, E.A. Ticianelli, J. Electrochem. Soc. 157 (2010) B697–B704.
[40] M.H. Atwan, D.O. Northwood, E.L. Gyenge, Int. J. Hydrogen Energy 32 (2007) 3116–3125.
[41] E. Sanli, H. Celikkan, B.Z. Uysal, M.L. Aksu, ECS Trans. 5 (2007) 137–145.
[42] E. Sanlı, H. Çelikkan, B. Zühtü Uysal, M.L. Aksu, Int. J. Hydrogen Energy 31 (2006) 1920–1924.
[43] B.H. Liu, Z.P. Li, S. Suda, J. Electrochem. Soc. 150 (2003) A398–A402.
[44] J. Ma, Y. Sahai, R.G. Buchheit, J. Power Sources 195 (2010) 4709–4713.
[45] D.M. Santos, C.A. Sequeira, ECS Trans. 16 (2009) 123–137.
[46] E. McCafferty, Introduction to Corrosion Sciences, Springer, New York, USA, 2010.
[47] C. Celik, F.G. Boyaci San, H.I. Sarac, J. Power Sources 185 (2008) 197–201.
[48] J. Zhi-fang, D. Dong-hong, S. Yan-ping, Battery Biomonthly 133 (2008).
[49] M.D. Hampton, D.V. Shur, S.Y. Zaginaichenko, V.I. Trefilov, Hydrogen Materials Science and Chemistry of Metal Hydrides, Kluwer Academic Publishers, Dodrecht, The Netherlands, 2002.
[50] H.A. Kiehne, Battery Technology Handbook, second ed., Expert Verlag GmbH, Renningen-Malsheim, Germany, 2003.
[51] L. Wang, C. Ma, Y. Sun, S. Suda, J. Alloys Compounds 391 (2005) 318–322.
[52] L. Wang, C.-a. Ma, X. Mao, J. Alloys Compounds 397 (2005) 313–316.
[53] G. Selvarani, S.K. Prashant, A.K. Sahu, P. Sridhar, S. Pitchumani, A.K. Shukla, J. Power Sources 178 (2008) 86–91.
[54] J. Ma, Y. Liu, P. Zhang, J. Wang, Electrochem. Comm. 10 (2008) 100–102.
[55] R.K. Raman, A.K. Shukla, Fuel Cells 7 (2007) 225–231.
[56] R.K. Raman, A.K. Shukla, J. Appl. Electrochem. 35 (2005) 1157–1161.
[57] R.K. Raman, S.K. Prashant, A.K. Shukla, J. Power Sources 162 (2006) 1073–1076.
[58] B.H. Liu, S. Suda, J. Alloys Compounds 454 (2008) 280–285.
[59] Z.P. Li, B.H. Liu, K. Arai, S. Suda, J. Alloys Compounds 404-406 (2005) 648–652.
[60] S. Özkar, M. Zahmakıran, J. Alloys Compounds 404–406 (2005) 728–731.
[61] C. Wu, F. Wu, Y. Bai, B. Yi, H. Zhang, Mater. Lett. 59 (2005) 1748–1751.
[62] A. Tentorio, U. Casolo-Ginelli, J. Appl. Electrochem. 8 (1978) 195–205.
[63] J.M. Friedrich, C. Ponce-de-León, G.W. Reade, F.C. Walsh, J. Electroanal. Chem. 561 (2004) 203–217.
[64] C. Ponce de León, A. Kulak, S. Williams, I. Merino-Jiménez, F.C. Walsh, Catal. Today 170 (2011) 148–154.
[65] C.T.J. Low, M. de la Toba Corral, F.C. Walsh, Trans. Inst. Met. Finish. 89 (2011) 44–50.
[66] C.J. Patrissi, R.R. Bessette, Y.K. Kim, C.R. Schumacher, J. Electrochem. Soc. 155 (2008) B558–B562.
[67] K. Strasser, J. Power Sources 29 (1990) 149–166.
[68] H. Cheng, K. Scott, J. Electroanal. Chem. 596 (2006) 117–123.
[69] H. Cheng, K. Scott, J. Power Sources 160 (2006) 407–412.
[70] C. Ponce de León, F.C. Walsh, A. Rose, J.B. Lakeman, D.J. Browning, R.W. Reeve, J. Power Sources 164 (2007) 441–448.
[71] A. Verma, A.K. Jha, S. Basu, J. Power Sources 141 (2005) 30–34.
[72] H. Cheng, K. Scott, K.V. Lovell, J.A. Horsfall, S.C. Waring, J. Membr. Sci. 288 (2007) 168–174.
[73] J. Ma, N.A. Choudhury, Y. Sahai, R.G. Buchheit, Fuel Cells 11 (2011) 603–610.
[74] K. Wang, J. Lu, L. Zhuang, Catal. Today 170 (2011) 99–109.
[75] Z.P. Li, B.H. Liu, J.K. Zhu, S. Suda, J. Power Sources 163 (2006) 555–559.
[76] U.B. Demirci, Electrochim. Acta 52 (2007) 5119–5121.
[77] R. Jamard, A. Latour, J. Salomon, P. Capron, A. Martinent-Beaumont, J. Power Sources 176 (2008) 287–292.
[78] C. Celik, F.G. Boyaci San, H.I. Sarac, Int. J. Hydrogen Energy 35 (2010) 8678–8682.
[79] D. Umit B, J. Power Sources 169 (2007) 239–246.
[80] Q. Zhang, G.M. Smith, Y. Wu, Int. J. Hydrogen Energy 32 (2007) 4731–4735.
[81] C. Celik, F.G.B. San, H.I. Sarac, J. Power Sources 195 (2010) 2599–2603.
[82] S.J. Kim, J. Lee, K.Y. Kong, C. Ryul Jung, I.-G. Min, S.-Y. Lee, H.-J. Kim, S.W. Nam, T.-H. Lim, J. Power Sources 170 (2007) 412–418.
[83] C. Kim, K.-J. Kim, M.Y. Ha, J. Power Sources 180 (2008) 154–161.
[84] H. Yang, T.S. Zhao, Electrochim. Acta 50 (2005) 3243–3252.
[85] K.T. Park, U.H. Jung, S.U. Jeong, S.H. Kim, J. Power Sources 162 (2006) 192–197.
[86] W. Qian, D.P. Wilkinson, J. Shen, H. Wang, J. Zhang, J. Power Sources 154 (2006) 202–213.
[87] C. Kim, K.-J. Kim, M.Y. Ha, J. Power Sources 180 (2008) 114–121.
[88] A. Verma, S. Basu, J. Power Sources 168 (2007) 200–210.
[89] A.E. Sanli, M.L. Aksu, B.Z. Uysal, Int. J. Hydrogen Energy 36 (2011) 8542–8549.
[90] G. Rostamikia, M.J. Janik, J. Electrochem. Soc. 156 (2009) B86–B92.
[91] G. Rostamikia, M.J. Janik, Electrochim. Acta 55 (2010) 1175–1183.
[92] G. Rostamikia, A.J. Mendoza, M.A. Hickner, M.J. Janik, J. Power Sources 196 (2011) 9228–9237.
[93] Y. Wu, M.T. Kelly, J.V. Ortega, Review of Chemical Processes for the Synthesis of Sodium Borohydride, Millenium Cell Inc, 2004.
[94] A.E. Sanli, i. Kayacan, B.Z. Uysal, M.L. Aksu, J. Power Sources 195 (2010) 2604–2607.
[95] E.L. Gyenge, C.W. Oloman, J. Appl. Electrochem. 28 (1998) 1147–1151.
[96] H.B.H. Cooper, Electrolytic Process for the Production of alkali Borohydrides, in, vol. US Patents 3734842, 1973.
[97] H. Sharifian, J.S. Dutcher, Production of Quaternary Ammonium and Quaternary Phosphonium Borohydrides, in, vol. US Patent 4904357, 1990.
[98] C.H. Hale, H. Sharifian, Production of Metal Borohydride and Organic Onium Borohydrides, in, vol. US Patent 4931154, 1990.
[99] Y. Sun, Z. Liang, Electrochemical Process for Preparing Borohydride, in, vol. CN Patent Appl. 1396307A, 2003.
[100] A.A. Shah, K.H. Luo, T.R. Ralph, F.C. Walsh, Electrochim. Acta 56 (2011) 3731–3757.
[101] A.A. Shah, M.J. Watt-Smith, F.C. Walsh, Electrochim. Acta 53 (2008) 8087–8100.
[102] W. Jung-Ho, J. Power Sources 161 (2006) 1–10.
[103] V. Grinberg, N. Mayorova, A. Pasynskii, Russ. J. of Electrochem. 45 (2009) 1321–1326.
[104] C. Lamy, C. Coutanceau, J.-M. Leger, The direct ethanol fuel cell: a challenge to convert bioethanol cleanly into electric energy, in: Catalysis for Sustainable Energy Production, Wiley-VCH Verlag GmbH & Co. KGaA, 2009, pp. 1–46.
[105] W. Vielstich, A. Lamm, H.A. Gasteiger, Fundamentals, technology and applications, in: Handbook of Fuel Cells, vol. 1–4, Wiley, 2003.
[106] G. Hoogers, Fuel Cell Technology Handbook, CRC Press, Florida, USA, 2003.
[107] F. Walsh, A First Course in Electrochemical Engineering, RSC Publishing, Cambridge, UK, 1993.
[108] Q. Zhang, G. Smith, Y. Wu, R. Mohring, Int. J. Hydrogen Energy 31 (2006) 961–965.
[109] M.C.S. Escaño, E. Gyenge, R.L. Arevalo, H. Kasai, J. Phys.Chem. C 115 (2011) 19883–19889.